

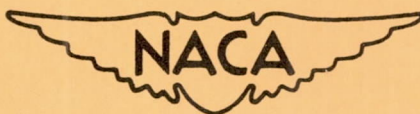
NATIONAL ADVISORY COMMITTEE FOR AERONAUTICS

TECHNICAL NOTE 4044

GROUND EFFECTS ON THE LONGITUDINAL CHARACTERISTICS OF TWO MODELS WITH WINGS HAVING LOW ASPECT RATIO AND POINTED TIPS

By Donald A. Buell and Bruce E. Tinling

Ames Aeronautical Laboratory
Moffett Field, Calif.



Washington

July 1957

TECHNICAL NOTE 4044

GROUND EFFECTS ON THE LONGITUDINAL CHARACTERISTICS
OF TWO MODELS WITH WINGS HAVING LOW
ASPECT RATIO AND POINTED TIPS¹

By Donald A. Buell and Bruce E. Tinling

SUMMARY

The ground effects on the longitudinal characteristics of two models with wings having low aspect ratio and pointed tips have been determined from wind-tunnel tests at Reynolds numbers from 2.5 to 10 million, using a flat plate to represent the ground. The first model had an aspect ratio of 2 and used trailing-edge flaps for longitudinal control. The flap hinge line had no sweepback and the flap chord was 25 percent of the wing chord. The second model had a triangular plan form of aspect ratio 3 and was equipped with flaps and a conventional tail.

The test results showed that the presence of the ground increased the lift-curve slope, decreased the drag due to lift, and increased the stick-fixed stability of the models. The latter effect was most pronounced on the model with the horizontal tail. The ground effect on the control-surface deflections for balance was small on the tailless model but was sizable on the tailed model. Control-surface hinge moments, measured only on the tailless model, were little affected at a given lift coefficient.

The experimentally determined ground effects on the lift and drag characteristics were generally underestimated by the theory of Tani, et al., at the higher lifts. When applied to the estimation of ground effects on the variation of pitching moment with lift coefficient of the tailed model, the theory had errors which tended to be compensating.

INTRODUCTION

The determination of effects of the ground on the aerodynamic characteristics of an airplane has, in the past, been concerned largely with straight wings of moderate to high aspect ratios. Consequently,

¹Supersedes recently declassified NACA RM A55E04 by Donald A. Buell and Bruce E. Tinling, 1955.

there is some question as to the applicability of the past work to many present-day high-speed airplanes. It was deemed appropriate to determine experimentally the ground effects on two models with wings having low aspect ratio and pointed tips and to compare the results with the available theory.

Longitudinal control of the airplane has been considered previously to be one of the more serious problems of ground proximity. Two types of longitudinal-control systems were represented on the models of the present investigation. The first model, having a wing of aspect ratio 2, used elevons (i.e., trailing-edge flaps) for longitudinal control. The second model, having a wing of aspect ratio 3, used a conventional tail.

The tests were made in the Ames 12-foot pressure wind tunnel at Reynolds numbers of from 2.5 to 10 million and at a Mach number of approximately 0.25. A flat plate spanning the wind tunnel was chosen to represent the ground. The disadvantage of a boundary-layer build-up along the plate, pointed out in reference 1 for example, was minimized insofar as was possible in the plate design. Limited pressure measurements were made to evaluate this discrepancy in the ground representation.

The experimentally determined ground effects were compared with those predicted by the theory of Tani, et al., (refs. 2 and 3). This theory had the advantages of simplicity with a certain amount of flexibility for adapting it to wings of low aspect ratio. The method is partially summarized and somewhat simplified in reference 4. The remainder of the applicable elements of the theory is summarized in an appendix to this report.

NOTATION

A aspect ratio, $\frac{b^2}{S}$

b wing span

c_D drag coefficient, $\frac{\text{drag}}{qS}$

c_{he} elevon hinge-moment coefficient, $\frac{\text{hinge moment}}{2qM_e}$

c_{ht} tab hinge-moment coefficient, $\frac{\text{hinge moment}}{2qM_t}$

C_L	lift coefficient, $\frac{\text{lift}}{qS}$
$C_{L_{\text{tail}}}$	increment of lift coefficient, C_L , due to the tail
C_m	pitching-moment coefficient about the moment center (specified in fig. 2), $\frac{\text{pitching moment}}{qS\bar{c}}$
$C_{m_{\text{tail}}}$	increment of pitching-moment coefficient C_m (at a constant angle of attack) due to the tail
c	wing chord measured parallel to the plane of symmetry
\bar{c}	wing mean aerodynamic chord, $\frac{2}{S} \int_0^{b/2} c^2 dy$
h	distance from the surface of the ground plate to the 0.25 \bar{c} (specified in fig. 2)
i_t	incidence of the horizontal tail with respect to the wing chord plane, deg
l_t	tail length, longitudinal distance from the moment center to the horizontal-tail hinge line
$\frac{L}{D}$	lift-drag ratio, $\frac{\text{lift}}{\text{drag}}$
M	free-stream Mach number
M_e	first moment of area of the exposed elevon behind the hinge line
M_t	first moment of area of the exposed tab behind the hinge line
q	free-stream dynamic pressure
R	Reynolds number, based on the wing mean aerodynamic chord
S	wing area
S_t	area of the horizontal tail
\tilde{V}	tail volume, $\frac{l_t}{\bar{c}} \frac{S_t}{S}$
y	distance perpendicular to the plane of symmetry

α	angle of attack, deg
δ_e	elevon deflection with respect to the wing-chord plane, measured in planes perpendicular to the elevon hinge line, deg
δ_f	flap deflection with respect to the wing-chord plane, deg
δ_t	tab deflection with respect to the elevon-chord plane, measured in planes perpendicular to the tab hinge line, deg
$\frac{\partial C_m}{\partial \alpha}$	horizontal-tail pitching-moment effectiveness, measured at a constant angle of attack
ϵ	effective downwash angle at the tail, deg
$\Delta\epsilon$	increase in effective downwash angle at the tail due to proximity of the ground, deg

APPARATUS AND MODELS

The ground representation is diagrammed in figure 1. The ground plate spanned the test section and was attached to the tunnel walls and to supporting struts on its lower side. The plate was made of 1/8-inch aluminum sheet fastened to an aluminum-angle frame with countersunk screws. The leading- and trailing-edge fairings were approximately elliptical. The leading-edge fairing was cambered to reduce the possibility of separation over the ground plate by keeping the stagnation point on the upper surface.

The model was supported by a sting which could be controlled in angle of attack and in elevation. A slot slightly larger than the sting was built into the trailing edge of the plate so that the model could be moved as close to the ground plate as desired at all positive angles of attack. The forward 16 inches of the slot were sealed with a flush plate for portions of the test.

Provision was made for determining the boundary-layer thickness on the ground plate, and the static pressures both on the plate and at several heights above the plate. The two locations of the rake used in the boundary-layer survey are shown in figure 1. The figure also shows the location of the row of orifices used to measure the static pressures on the plate. The static pressures above the plate were measured along a tube containing several sets of orifices. This tube was mounted on the model support in place of the model.

The geometry of the models is given in figure 2 and in tables I and II. The tailless model had a wing which was built around a steel spar. The forward part of the wing was made of a tin-bismuth alloy bonded to the

spar, and the rear part consisted of solid steel elevons and tabs attached by hinges and internal brackets. The elevon and tab on the right-hand side of the model were restrained from rotating about their hinge lines by strain-gage members of the cantilever bending type for the purpose of measuring hinge moments. The wing section was the NACA 0005-63 modified slightly to provide straight-line elements from the elevon hinge line to the trailing edge.

The tailed model had solid steel wing and tail surfaces. The wing was provided with single-slotted flaps attached with 1/4-inch-thick external brackets screwed to the lower surfaces. The ailerons, which were not deflected during the tests, were similarly supported. For the tests with flaps up, the ailerons and flaps were replaced by a solid insert with no slots or external supports. The fuselage could be shortened by the removal of a cylindrical portion, which was 6.5 inches in length. (See table II.)

Both models are pictured installed over the ground plate in figure 3.

The forces and moments on each model were measured on a 4-inch-diameter, four-component, strain-gage balance enclosed within the model fuselage. Provision was made for measuring the pressure inside the base of the model between the sting and the model.

TESTS

The tests were conducted in three parts: (1) boundary-layer surveys on the ground plate and static-pressure surveys on and above the ground plate (with no models installed), (2) force tests of the models in the presence of the ground plate, and (3) force tests of the models without the ground plate. The tests included measurement of the models' lift, drag, pitching moment, and hinge moments (the latter on the control surfaces of the tailless model only) with various control-surface and flap deflections. Most of the tests were made at a dynamic pressure of 80 pounds per square foot with the wind tunnel at atmospheric pressure. These test conditions correspond to a Mach number of 0.25 and Reynolds numbers of 3 million for the tailless model, and 2.5 million for the tailed model. Since the accurate measurement of drag characteristics was difficult at this low Reynolds number, some data were obtained at higher Reynolds numbers (8 million and 10 million for the tailless model and tailed model, respectively).

For most of the tests the angle of attack was varied from -4° to the mechanical limit of the model-support system (approximately 14° with the ground plate installed, 24° without the ground plate). With the ground plate installed, angles of attack up to 28° were reached by mounting the model on a bent sting and making the force tests at large angles separately

from those at small angles. At the smallest ground heights, the angle of attack was limited to that beyond which the model would collide with the plate (23° for the tailless model, 12° for the tailed model).

The pressure surveys were made with the static-pressure tube on the model support at heights above the ground plate roughly the same as those of the force tests. The boundary-layer survey was made with no model installed, while the static pressures along the plate were measured both during the pressure survey and during the force tests.

GROUND SIMULATION

The applicability of the data is, of course, limited by the accuracy with which the ground was simulated. The boundary layer on the plate is probably the first consideration in this respect. The boundary-layer survey (with no model installed) indicated the existence of a turbulent boundary layer with a displacement thickness which varied from $1/16$ inch at the station of the model's nose to approximately $1/8$ inch at the station of the maximum spanwise dimension of the wing. There was little effect of Reynolds number on the boundary-layer thickness within the range of Reynolds numbers of the tests. The assumption that the presence of the model did not greatly thicken the plate boundary layer is supported by the results of the static-pressure measurements on the plate. The static-pressure measurements indicated that the position of stagnation (on the upper surface near the leading edge) was unaffected by the presence of the model and that the pressure gradients induced by the model were small enough not to cause separation. On the basis of these measurements, the effects of the boundary layer were considered negligible.

The static-pressure survey showed evidence of a longitudinal pressure gradient in the tunnel air stream which was caused by local disturbances near the leading and trailing edges of the ground plate. Although the noses of the models extended into the region of the gradient caused by the leading edge of the plate, no buoyancy correction was applied to the drag data. The static pressures on the noses of the models at the smaller ground heights were lower than the free-stream value by about 3 percent at the smallest angles of attack and by about 1 percent at the largest angles of attack. The trailing-edge disturbance, which was of a smaller magnitude, was essentially compensated for (in the calculation of drag) by the base-pressure correction explained hereinafter.

CORRECTIONS TO DATA

The data were corrected for the induced effects of the tunnel walls resulting from lift on the model by the method of reference 5 as applied

to a circular tunnel. For the case of the model installed over the ground plate, a reflection plane was assumed at the surface of the ground plate and was represented by vortices of equal strength and at equal distances below the plane to those simulating the model lift. It was here convenient to approximate the tunnel shape by a circle whose area was twice that of the tunnel cross section above the ground plate. Values of the correction are as follows:

Tailed model			Tailless model		
$\frac{h}{c}$	$\frac{\Delta\alpha}{C_L}$	$\frac{\Delta C_D}{C_L^2}$	$\frac{h}{c}$	$\frac{\Delta\alpha}{C_L}$	$\frac{\Delta C_D}{C_L^2}$
∞	0.30	0.0045	∞	0.26	0.0046
1.25	.07	.0012	1.25	.11	.0018
.90	.04	.0007	.75	.04	.0006
.60	.02	.0003	.50	.01	.0002

Calculations made by the method of reference 6 indicated the pitching-moment correction to be negligible.

Corrections applied to the data to account for the effects of constriction due to the tunnel walls were calculated by the method of reference 7. The value of the correction to dynamic pressure was less than 1/2 percent.

The interference between the model and the sting (and the ground-plate trailing edge) was partially compensated for by a correction to the drag, using the base pressure measured at the model base. The drag data as corrected are those of a model with free-stream static pressure on its base.

No corrections were applied to the data to account for deflection of the control surfaces under aerodynamic load (resulting from bending of the restraining gage members). A static calibration on the elevon and tab of the tailless model indicated the change in angle to be less than 0.2° for the elevon and 0.1° for the tab when the largest hinge moments imposed during the tests were applied.

RESULTS AND DISCUSSION

Tailless Model

The effects of ground proximity on the longitudinal characteristics of the tailless model with control surfaces neutral are shown in figure 4. As would be anticipated from theory and from previous experimental results, the proximity to the ground increased the lift-curve slope and decreased

the drag due to lift. The slope of the pitching-moment curves became more negative, indicating an increase in stability as the ground was approached.

The effects of ground proximity on the lift and pitching-moment characteristics of the model with various elevon and tab deflections are shown in figure 5. It may be seen from the figure that the ground effects on the slopes of the lift and pitching-moment curves were about the same for all the control-surface deflections. There was some effect of ground proximity on the elevon deflection required to balance the model (i.e., to make $C_m = 0$). However, the elevon deflection for balance was changed less than 1° by the ground in all cases. Figure 6 shows the ground effects on the drag characteristics of the model with no tab deflection. Here, again, there was little change in the ground effects with changing elevon deflection. A comparison of figures 5(a) and 6 with figure 4 indicates that the ground effects were approximately the same at Reynolds numbers of 3 and 8 million.

The lift and drag characteristics of the tailless model balanced in pitch by the elevons are summarized in figure 7. By comparing figure 7 with figures 5(a) and 6 it can be seen that the ground effects on the lift and drag characteristics of the model in balance were little different from those with a constant elevon deflection at the same lift coefficient.

The hinge-moment characteristics of the elevon and tab are given in figure 8. Most of the data indicate that there was little ground effect on these hinge-moment coefficients at a given lift coefficient. The elevon characteristics for -5° deflection show some discrepancies, but these are believed to be due to temporarily faulty instrumentation. The floating tendencies of the control surfaces are defined as the rate of decrease of hinge-moment coefficient with increasing angle of attack. It is concluded that the floating tendencies were increased by proximity to the ground because of the increase in lift-curve slope (fig. 5).

Figure 9 demonstrates the accuracy with which the lift and drag characteristics of the model near the ground could be predicted by the theory of Tani, et al. The theory is based on the hypothesis that the effects of the ground on a wing are the same as the effects which would be induced by the flow about an identical wing symmetrically disposed with respect to the actual wing on the opposite side of the ground plane. The interference between the two wings can then be calculated by the methods employed with biplanes. (The theory is discussed in the appendix.) The theory underestimated the ground effects at the higher lifts. The divergence between the theory and experiment as the lift increased is possibly a result of using an inadequate method to determine a mean-weighted value of the chord divided by ground height, which is the basic parameter used in the theory. This parameter is calculated using the span load distribution as a weighting factor with the assumption that the span load distribution is elliptical. The theory might have provided a better estimate if account had been taken of the change in span loading caused

by flow separation which probably progressed inward from the wing tips with increasing lift. Tani's method of predicting pitching-moment changes near the ground is not directly applicable to swept wings, and no attempt was made to adapt it.

Tailed Model

The ground effects on the longitudinal characteristics of the tailed model with its horizontal tail removed are shown in figure 10 to be similar to those on the tailless model (fig. 4). The magnitude of the effects was very nearly the same for a given h/\bar{c} .

The tail-off characteristics of the tailed model (at a Reynolds number of 2.5 million) with and without flap deflection are presented in figure 11. The ground effects shown for the flaps-up configuration are similar to those measured at the higher Reynolds number (fig. 10). The slight differences in the mean values of the measured ground effects are attributed to differences in fuselage length, the fuselage being shortened for the tests at high Reynolds number in an effort to extend the angle-of-attack range.

The theory was used to determine the lift and drag characteristics of the model at the two lower ground heights, with the results shown in figure 12. The theory generally underestimated the ground effects at the higher lifts, as it did with the first model.

A ground effect of more importance to the static-longitudinal-stability and control problem is shown by the data in figures 13 through 15, where the tail-on pitching-moment characteristics are given for various ground heights. As the model approached the ground, it became more stable (stick-fixed) with, generally, a more negative tail incidence required for balance. This increment in tail incidence was as much as 8° with flaps down when the ground height was reduced from ∞ to $0.60\bar{c}$ (fig. 15).

The data taken with the forward part of the slot in the ground plate sealed (see figs. 13 and 14) indicate that the slot had only a small effect. Also, the effect was presumably smaller at those tail incidences at which the tail was more lightly loaded (i.e., at which the pitching-moment coefficients were closer to those of the tail-off configuration).

The experimentally determined ground effects on the lift and drag characteristics of the model in a balanced condition are shown in figure 16. By comparing this figure with figure 11, it can be seen that the addition of the tail to balance the model caused only minor changes in the ground effects on the lift and drag characteristics over most of the lift range.

The theoretical pitching-moment characteristics of the model with tail on, shown in figures 13 and 14, are a composite of the data taken with the ground plate removed, and of the ground effects calculated by the method detailed in the appendix. In essence, the calculation consists of estimating the downwash changes and the consequent changes in pitching moment and lift contributed by the tail, along with the previous calculation of changes in wing lift characteristics. Since this estimation is made at a given angle of attack rather than lift coefficient, little error was incurred (for this model) by ignoring the ground effects on the wing and fuselage pitching moments (shown in fig. 11). The estimation of ground effects, flaps down, was not attempted at low lifts because the tail was apparently stalled at most of the tail incidences tested, and the relation between pitching moment and tail angle of attack was no longer definitely known.

The approximations involved in estimating the pitching-moment characteristics near the ground can be assessed for the flaps-up configuration from figures 17 and 18. The experimental downwash was computed from the data using the relation

$$\epsilon = \alpha + it - \frac{C_{m\text{tail}}}{\partial C_m / \partial it}$$

The elementary method for estimating downwash used by Tani gave a reasonable estimate of downwash angle ϵ and of the change in downwash angle $\Delta\epsilon$ caused by the ground (see fig. 17). The values at 0° angle of attack indicate an experimental discrepancy between downwash angles with the ground plate and those without the ground plate of about 0.5° . This was, of course, reflected as an apparent error in estimating the pitching-moment characteristics near the ground. A larger error was incurred by assuming no effect of ground proximity on $\partial C_m / \partial it$. However, this ground effect would have been difficult to estimate since it stemmed not only from a change in lift-curve slope of the tail, but also from changes in the dynamic pressure at the tail. The latter ground effect was partly a result of the reduction in the velocity at the lifting surfaces caused by the ground, and partly a result of a change in the height of the wing wake with its local velocity variations. The proximity of the tail to the trailing edge of the ground plate was also responsible for some changes in dynamic pressure at the tail, but the pressure surveys indicated that these were relatively small.

The accuracy of estimating the lift characteristics of the complete model was little affected by the errors involved in estimating the tail lift, as can be seen by comparing figure 18 with figure 12(a). (Fig. 18 presents typical data for which the tail was not stalled.)

Figures 19 and 20 show values for the factors of importance in estimating ground effects when the flaps were down. For this configuration,

the simple method used by Tani for predicting downwash was somewhat modified to take account of the concentration of lift over the flap span. (See Appendix.) It is apparent that the estimated downwash angles fell far short of the experimental values, as did also the estimated changes in wing downwash caused by the ground. As a consequence, the pitching-moment increments calculated therefrom were smaller than the experimental values. Also, a comparison of figure 12(a) with figure 20 shows that the estimation of the ground effect on the lift characteristics of the model with flaps down differed somewhat more from experimental values when the estimated tail lift was included. However, the underestimation of the pitching-moment increments (due to the ground) tend to compensate for the underestimation of the lift increments when the theory is used to predict the variation of pitching-moment coefficient with lift coefficient as was done in figure 14.

CONCLUDING REMARKS

Tests of two models with wings having low aspect ratio and pointed tips have shown that proximity to a plate representing the ground increased the lift-curve slope and decreased the drag due to lift. The ground also increased the stick-fixed stability of the models, this effect being most pronounced on the model with a horizontal tail. The elevon deflections required to balance the tailless model were changed less than 1° as the ground height was reduced from ∞ to $0.50\bar{c}$, whereas the incidence of the tail required to balance the tailed model, with flaps down, was decreased as much as 8° when the ground height was reduced from ∞ to $0.60\bar{c}$. The hinge-moment coefficients of the control surfaces on the tailless model were little affected by the ground at a given lift coefficient.

The Tani theory generally underestimated the ground effects on the lift and drag characteristics of these models at high lifts. When applied to the estimation of the ground effects on the variation of pitching-moment coefficient with lift coefficient of the tailed model, the theory had errors which tended to be compensating.

Ames Aeronautical Laboratory
National Advisory Committee for Aeronautics
Moffett Field, Calif., May 4, 1955.

APPENDIX

APPLICATION OF THE TANI METHOD FOR ESTIMATING
GROUND EFFECTS

A summary and discussion of the method of Tani, et al., (refs. 2 and 3) for estimating the effect of the ground on the lift and drag characteristics of an airplane is presented in reference 4, omitting, however, his proposed method for establishing a representative mean value for chord, thickness ratio, and height above the ground. To apply the theory to swept wings of low aspect ratio, it was deemed necessary to use some such means for establishing a representative ground height. Therefore, the following relations similar to those from reference 2 were used, together with the equations and chart of reference 4, for estimating ground effects for the models of the present report; the average chord is given by the expression

$$\int_0^1 c \, d\eta = \frac{S}{b}$$

and the mean weighted value of c/H is expressed as

$$\frac{4}{\pi} \int_0^1 \frac{c}{H} \sqrt{1 - \eta^2} \, d\eta$$

with

c the wing chord at span station η

H the height from the ground to the quarter-chord point at the span station η

η a ratio of distance from the plane of symmetry to semispan, $y/(b/2)$

The use of these relations was generally of more importance to the result than the inclusion of such refinements as the effects of wing thickness.

Tani's method for estimating the ground effects on the tail (ref.3) are summarized next, together with a modification to the method for use with flaps down. It was desired to estimate the ground effects on the pitching moment contributed by the tail, at a given angle of attack. Let $(\Delta C_m)_{tail} = \Delta C_{m1} + \Delta C_{m2}$ = increase in C_m due to ground effects on the tail where

$$\Delta C_{m_1} = - \frac{\partial C_m}{\partial it} \Delta \epsilon$$

$$\Delta C_{m_2} = -\Delta C_{L_t} \bar{V}$$

The first increment in pitching-moment coefficient ΔC_{m_1} is the larger of the two, being composed of the term $\partial C_m / \partial it$ that is taken from experimental data with no ground plate (the ground effect on $\partial C_m / \partial it$ is assumed to be negligible) and a downwash term representing the ground-induced change in wing downwash at the tail position. The ground is simulated by the lifting vortices of an image of the wing and the downwash term is calculated as follows: In general,

$$\epsilon = J(\xi, \zeta) C_{L_w}$$

where

$$J(\xi, \zeta) = \frac{57.3}{2\pi A} \left[\frac{\xi}{\sqrt{k^2 + \xi^2 + \zeta^2}} \left(\frac{1}{\xi^2 + \zeta^2} + \frac{1}{k^2 + \zeta^2} \right) + \frac{1}{k^2 + \zeta^2} \right]$$

in degrees. Near the ground, the increase in downwash caused by the ground is expressed as

$$\Delta \epsilon = J(\xi, \zeta) \Delta C_{L_w} - J(\xi, \zeta') (C_{L_w} + \Delta C_{L_w})$$

The meaning of the geometric terms is illustrated in figure 21. The term C_{L_w} is the wing lift coefficient, measured with no ground plate, while ΔC_{L_w} is the calculated increase in wing lift (at a given angle of attack) caused by the ground. The fuselage lift was included in the term C_{L_w} . The lift distribution was assumed to be elliptical; for this condition, k is taken as $\pi/4$.

The second increment in pitching-moment coefficient ΔC_{m_2} results from a change in tail lift which occurs for the same reasons that the wing lift changes near the ground. In the case of the tail, only the major ground effect is considered, this being the induced angle of attack caused by the trailing vortices of the image tail. This induced angle of attack is then transformed into an increase in tail lift coefficient, expressed as

$$\Delta C_{L_t} = - \left(\frac{57.3 \sigma_t}{\pi A_t} \right) C_{L_t} \frac{\partial C_m}{\partial it} \frac{1}{\bar{V}}$$

In this relation, the induced upwash factor σ can be approximated, as in reference 4 for the wing, as

$$\sigma_t = e^{-2.48(2ht/bt)^{0.768}}$$

A_t is the tail aspect ratio; the other geometric terms are described in figure 21. The tail lift coefficient is approximated as

$$C_{L_t} = -\frac{1}{V} \left(C_{m_{tail}} + \Delta C_{m_1} \right)$$

where $C_{m_{tail}}$ is the increment of pitching-moment coefficient due to the tail and is taken from the experimental data with no ground plate.

The change in lift coefficient of the model resulting from the effects of the ground at the tail is expressed as

$$(\Delta C_L)_{tail} = -\frac{(\Delta C_m)_{tail}}{l_t/\bar{c}}$$

The above relations for estimating downwash at the tail were inadequate for the case of flaps down. Here, the angle of downwash was assumed to be the sum of two components (as in ref. 8), the first stemming from the flaps-up lift distributed over the original wing vortex span, and the second stemming from the lift due to flap deflection distributed over the flap vortex span. With the assumption that the flap lift had an elliptical distribution, it was possible to calculate a value $[J(\xi, \zeta)]_f$ for that wing area ahead of and including the flaps. Then,

$$\epsilon_{flaps\ down} = [C_{L_w} J(\xi, \zeta)]_{flaps\ up} + \Delta C_{L_{W_f}} [J(\xi, \zeta)]_f$$

where $\Delta C_{L_{W_f}}$ is the increase in lift coefficient resulting from flap deflection. It was noted that by suitable factoring, $\Delta C_{L_{W_f}}$, ξ , ζ , and A for the flapped area could be kept in terms of the complete-wing area and span if k were multiplied by the ratio of flap span to wing span before calculating $[J(\xi, \zeta)]_f$. The tail was assumed to be sufficiently immersed in the downwash from the flaps to make the calculated value a representative one. The increment in downwash, $\Delta\epsilon$, due to the ground was then calculated using an adjusted downwash parameter

$$J(\xi, \zeta)_a = \frac{\epsilon_{flaps\ down}}{(C_{L_w})_{flaps\ down}}$$

in place of $J(\xi, \zeta)$ in the original expression for $\Delta\epsilon$. The value of $J(\xi, \zeta')$ was similarly adjusted, so that

$$\begin{aligned} (\Delta\epsilon)_{\text{flaps down}} &= J(\xi, \zeta)_a (\Delta C_{L_w})_{\text{flaps down}} - \\ &J(\xi, \zeta')_a (C_{L_w} + \Delta C_{L_w})_{\text{flaps down}} \end{aligned}$$

REFERENCES

1. Le Sueur, Maurice: Ground Effect on the Take-off and Landing of Airplanes. NACA TM 771, 1935.
2. Tani, Itiro, Taima, Masuo, and Simidu, Sodi: The Effect of Ground on the Aerodynamic Characteristics of a Monoplane Wing. Rep. No. 156 (vol. XIII, no. 2), pp. 23-76, Aero. Res. Inst., Tokyo Imperial Univ., Sept. 1937.
3. Tani, Itiro, Itokawa, Hideo, and Taima, Masuo: Further Studies of the Ground Effect on the Aerodynamic Characteristics of an Aeroplane with Special Reference to Tail Moment. Rep. No. 158 (vol. XIII, no. 4), pp. 117-145, Aero. Res. Inst., Tokyo Imperial Univ., Nov. 1937.
4. Wetmore, J. W., and Turner, L. I., Jr.: Determination of Ground Effect from Tests of a Glider in Towed Flight. NACA Rep. 695, 1940.
5. Silverstein, Abe, and White, James A.: Wind Tunnel Interference With Particular Reference to Off-Center Positions of the Wing and to the Downwash at the Tail. NACA Rep. 547, 1935.
6. Sivells, James C., and Salmi, Rachel M.: Jet-Boundary Corrections for Complete and Semispan Swept Wings in Closed Circular Wind Tunnels. NACA TN 2454, 1951.
7. Herriot, John G.: Blockage Corrections for Three-Dimensional-Flow Closed-Throat Wind Tunnels, With Consideration of the Effect of Compressibility. NACA Rep. 995, 1950. (Formerly NACA RM A7B28)
8. Silverstein, Abe, Katzoff, S., and Bullivant, Kenneth W.: Downwash and Wake Behind Plain and Flapped Airfoils. NACA Rep. 651, 1939.

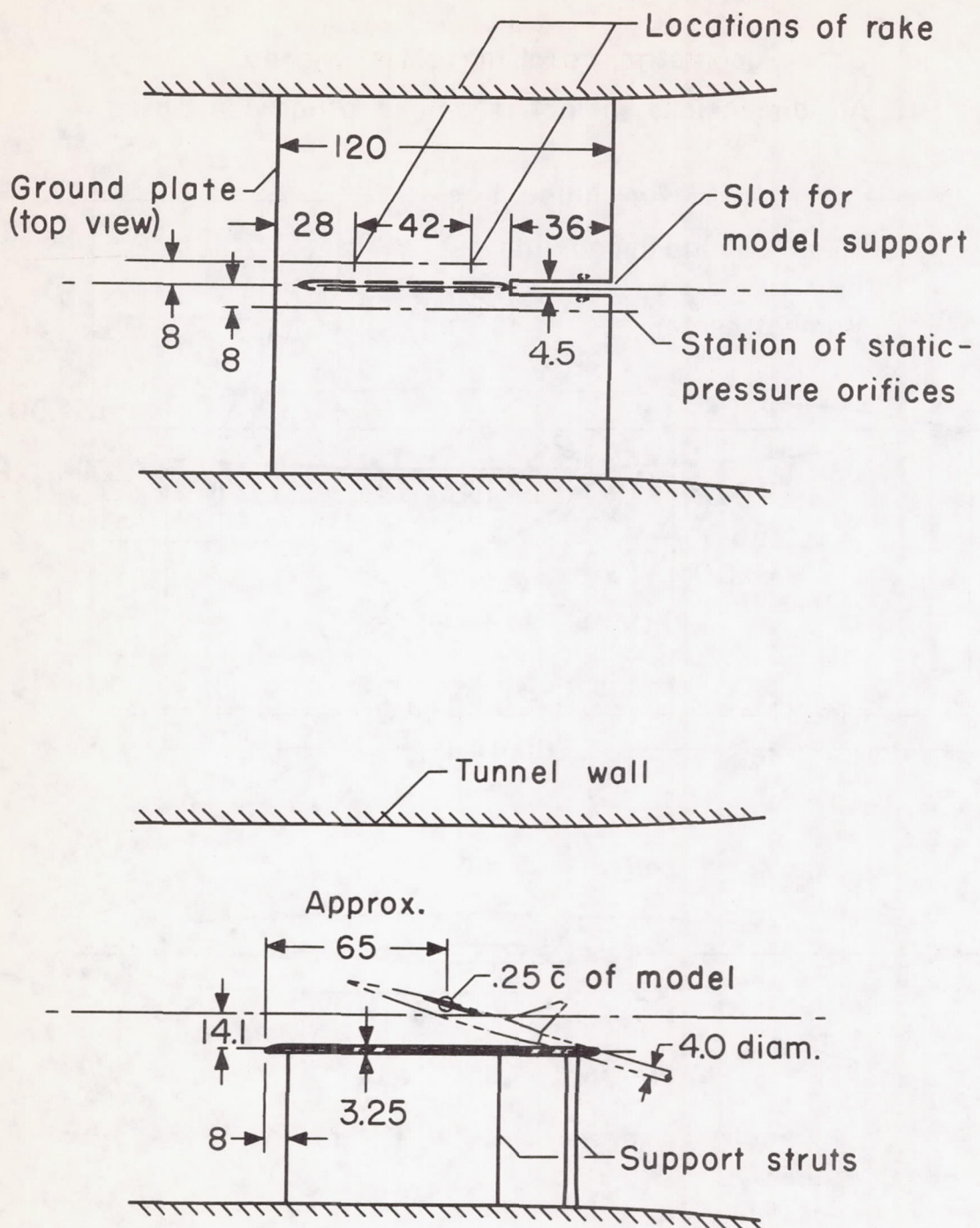
TABLE I.-- GEOMETRIC PROPERTIES OF THE MODELS

Tailless model	Tailed model
Wing	Wing
Aspect ratio	2.00
Sweep, 0.25 chord line, deg	45.0
Area, sq ft	4.014
Taper ratio	0
Section, streamwise (leading edge to elevon hinge line)	NACA 0003.5-63
Incidence, deg	0
Dihedral, deg	0
Elevon	Flaps
Chord, fraction of wing chord	Span, fraction of wing span 0.584
0.250	Area, fraction of total wing area 0.111
Exposed area, fraction of exposed wing area	Ailerons
0.25	Area, fraction of total wing area 0.067
First moment of area of exposed elevon behind hinge line, cu ft	Horizontal tail
0.0699	Aspect ratio
Tab	Area, sq ft
Chord, fraction of elevon chord	0.867
0.250	Taper ratio
Exposed span, fraction of exposed elevon span	0.33
0.40	Section NACA 0004-64
Exposed area, fraction of exposed elevon area	Vertical tail
0.25	Aspect ratio (geometric) 1.50
First moment of area of exposed tab behind hinge line, cu ft	Area (to fuselage center line), sq ft
0.00321	1.067
Fuselage	Taper ratio
Fineness ratio	0.16
Base area, sq ft	Section NACA 0003.5-64
	Fuselage
	Fineness ratio
	12.0
	Base area, sq ft
	0.13

TABLE II.- FUSELAGE COORDINATES

Tailless model		Tailed model	
Distance from nose, in.	Radius, in.	Distance from nose, in.	Radius, in.
0	0	0	0
5.00	1.06	5.00	.80
10.00	1.69	10.00	1.44
15.00	2.16	15.00	1.94
20.00	2.52	20.00	2.32
25.00	2.78	25.00	2.60
30.00	2.95	30.00	2.79
35.00	3.04	35.00	2.90
40.00	3.06	40.00	2.97
45.00	2.99	45.00	2.99
50.00	2.84	^a 51.25	^a 3.00
55.00	2.61	^a 57.75	^a 3.00
60.44	2.25	61.75	2.99
		65.75	2.90
		69.75	2.67
		72.00	2.44

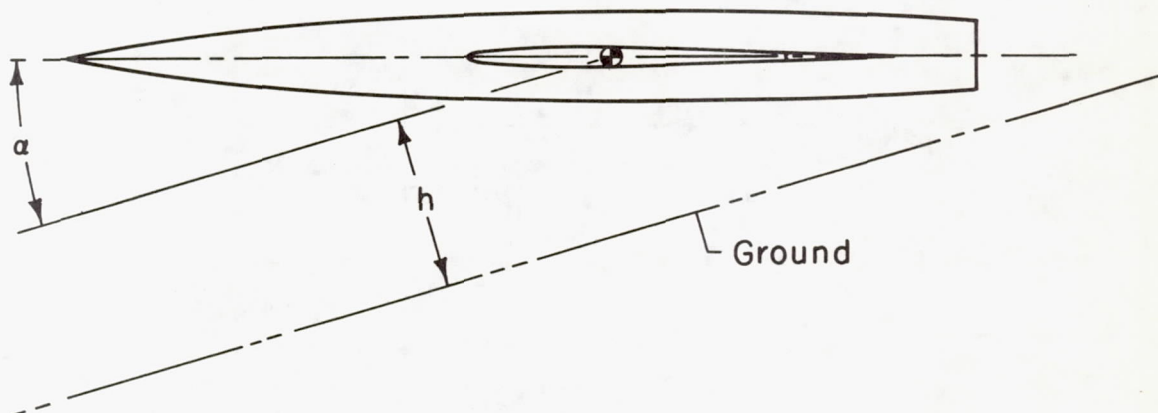
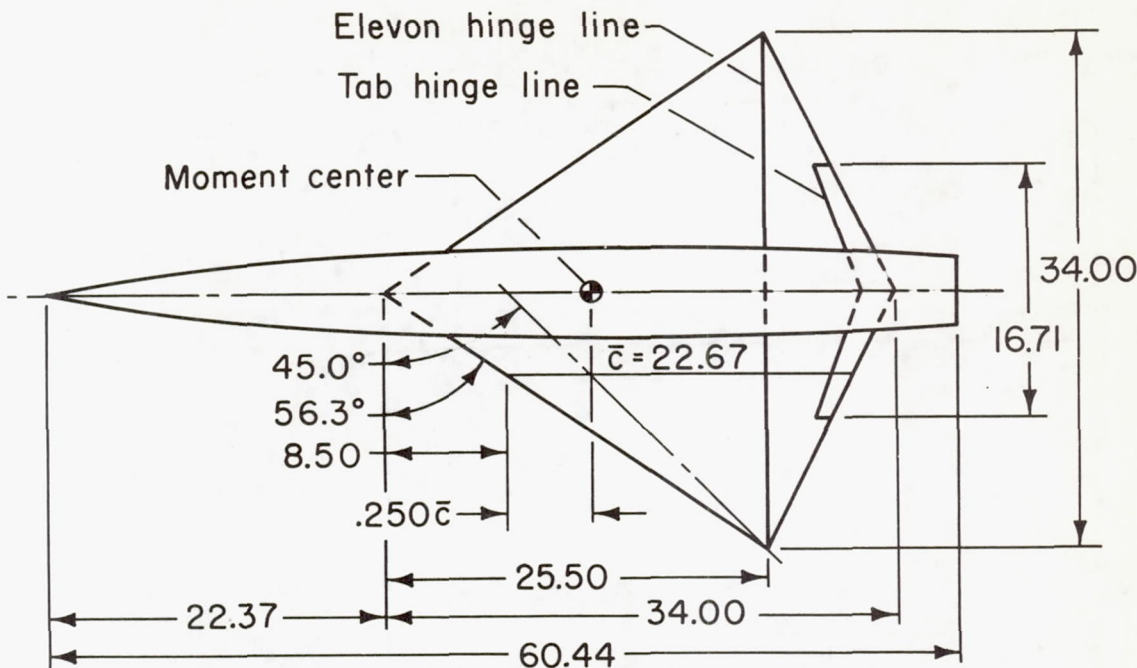
^aRemovable section



All dimensions in inches unless otherwise noted

Figure 1.- Diagram of the ground-plate installation.

Other geometric data in tables I and II
 All dimensions in inches unless otherwise noted

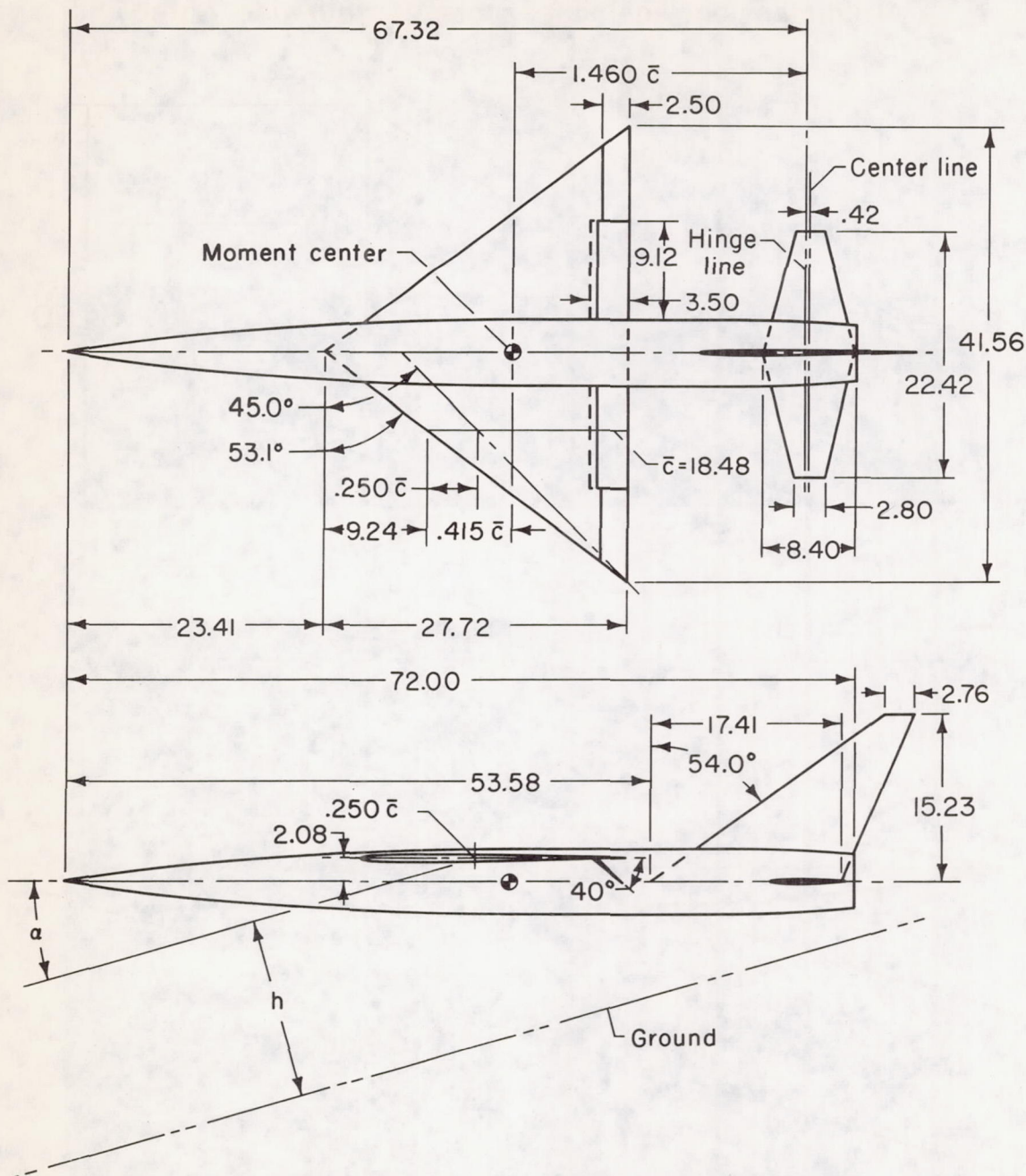


(a) Tailless model.

Figure 2.- Geometry of the models.

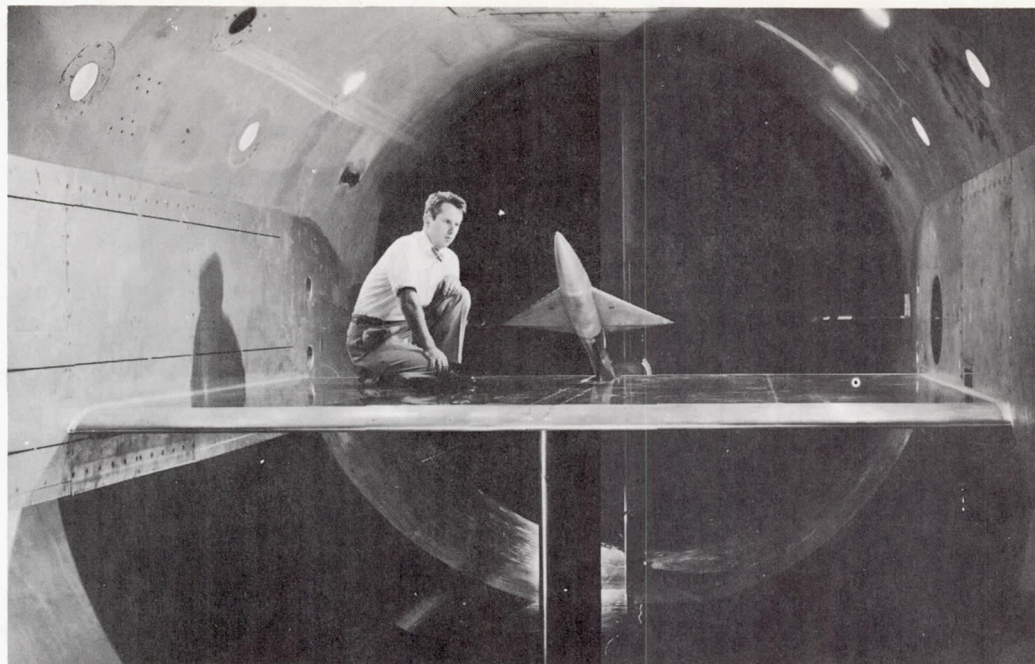
Other geometric data in tables I and II

All dimensions in inches unless otherwise noted



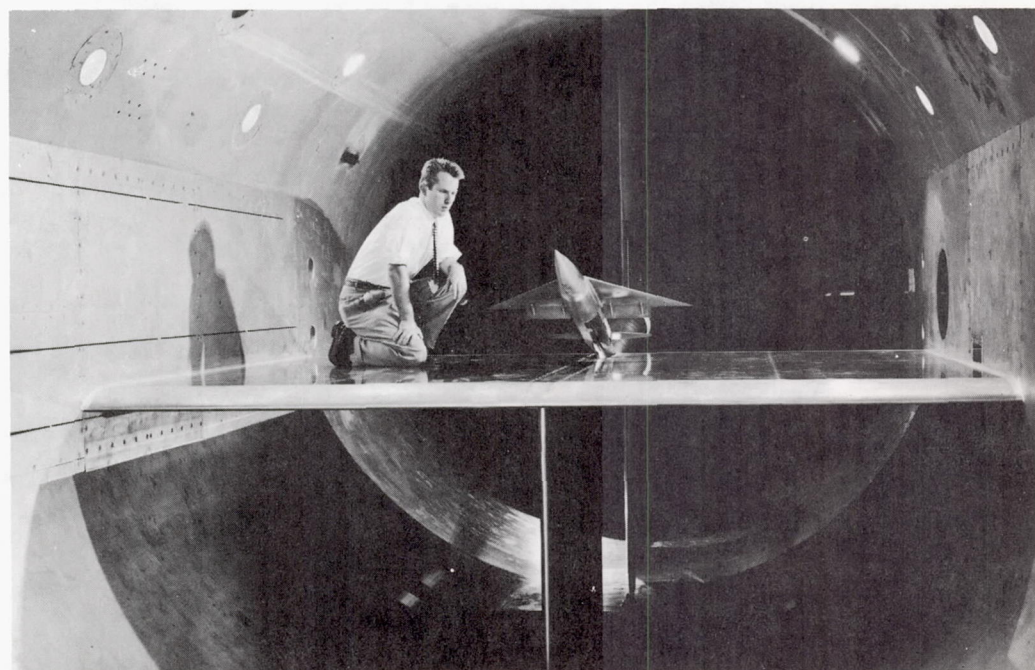
(b) Tailed model.

Figure 2.- Concluded.



(a) Tailless model.

A-19490



(b) Tailed model.

A-19501

Figure 3.- The models and ground plate installed in the wind tunnel.

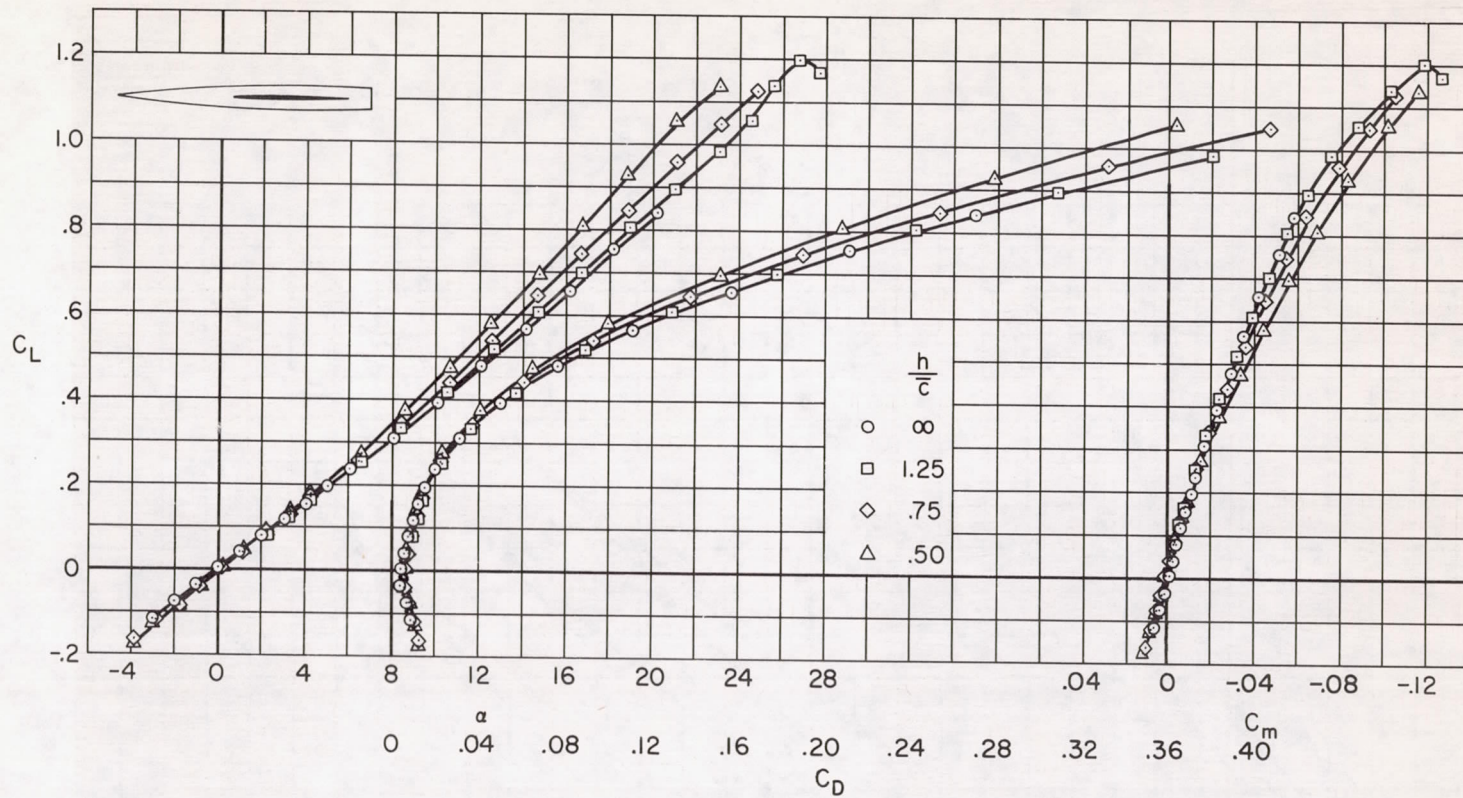


Figure 4.- The effect of ground height on the longitudinal characteristics of the tailless model;
 $R = 8$ million, $\delta_t = 0^\circ$, $\delta_e = 0^\circ$.

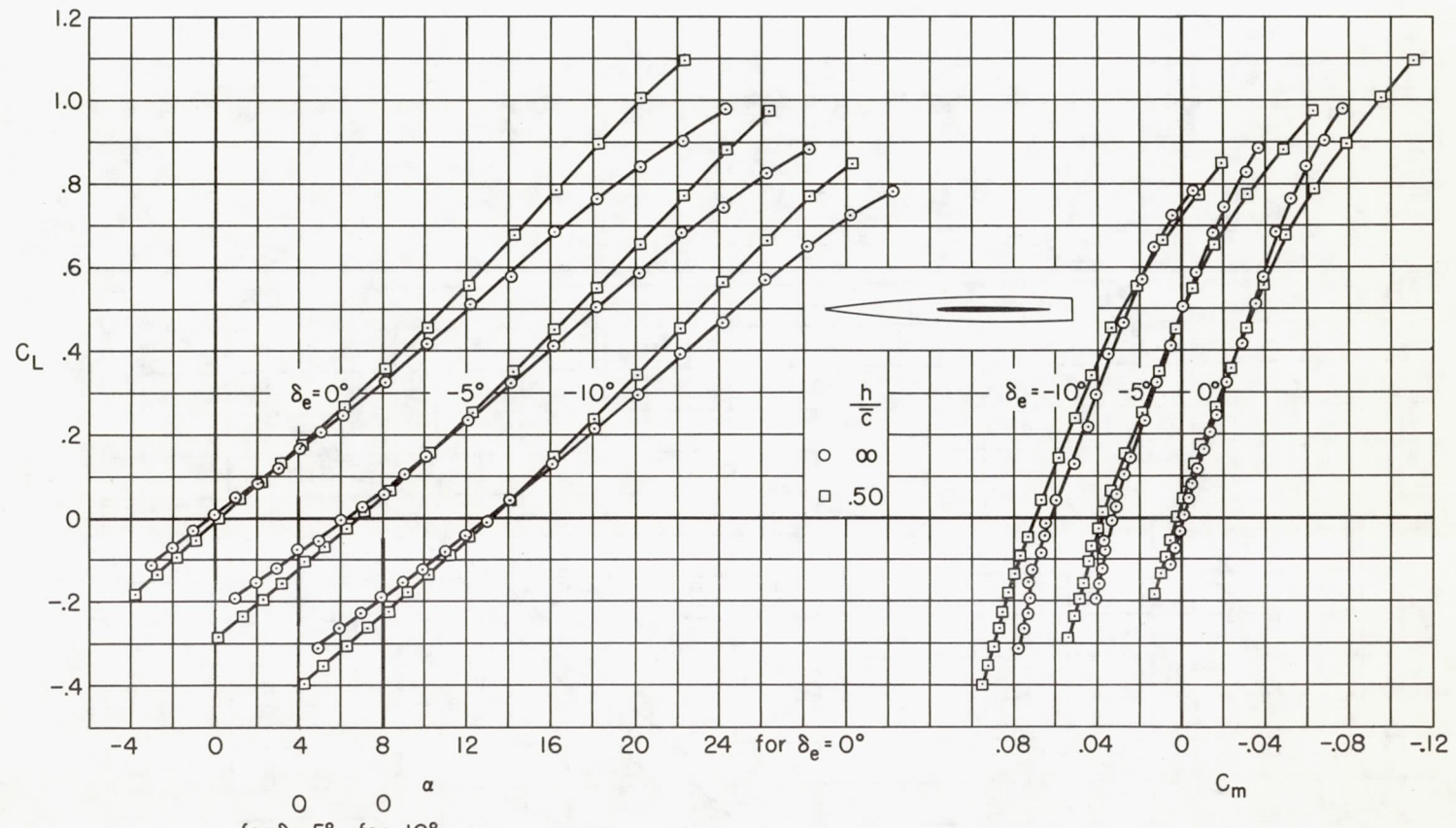
(a) $\delta_t = 0^\circ$

Figure 5.- The effect of ground height on the lift and pitching-moment characteristics of the tailless model; $R = 3$ million.

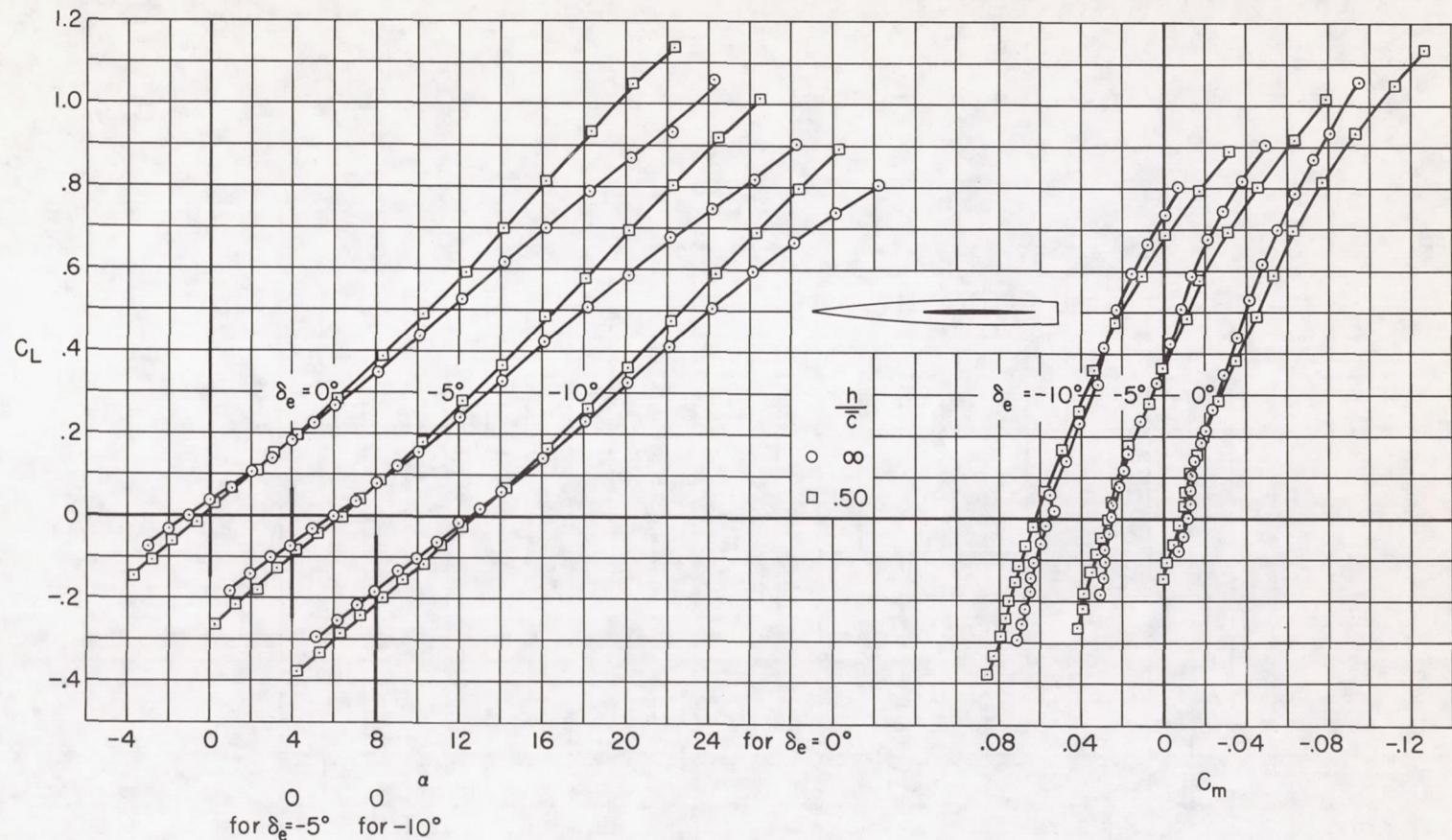
(b) $\delta_t = 5^\circ$

Figure 5.- Concluded.

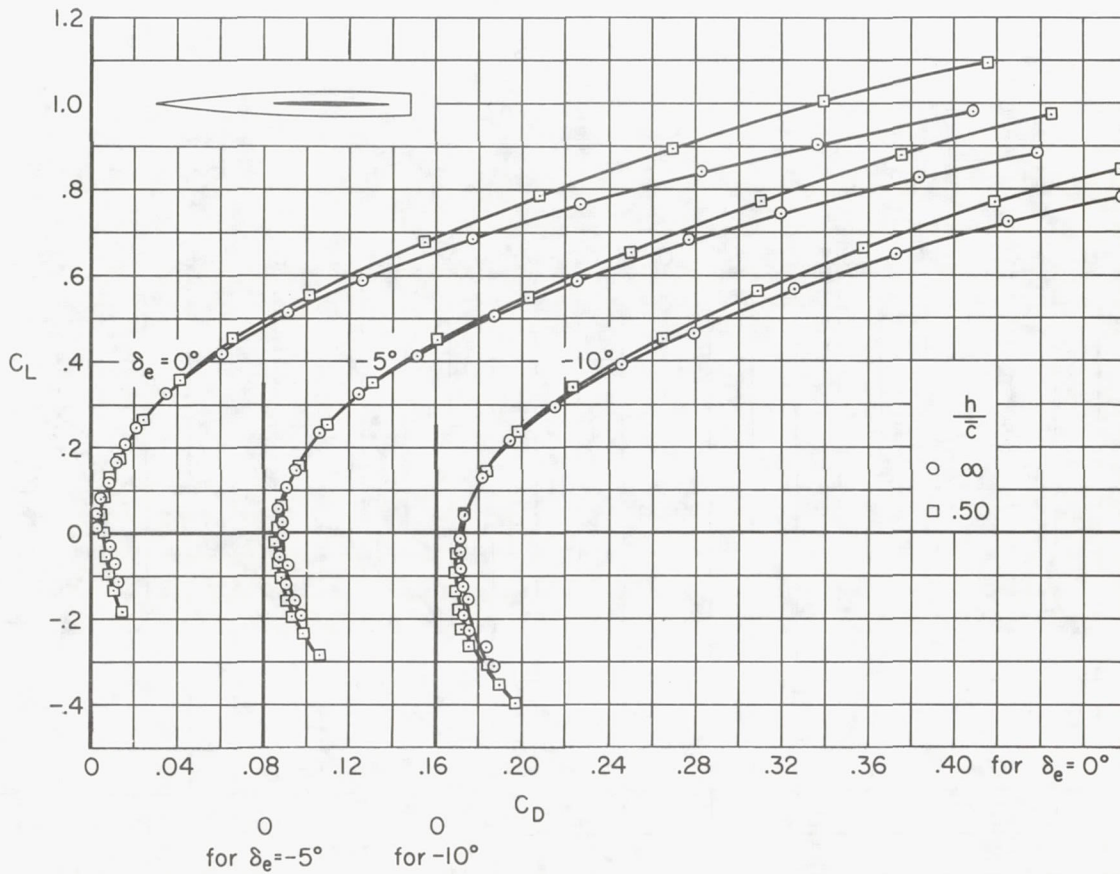


Figure 6.- The effect of ground height on the drag characteristics of the tailless model;
 $R = 3$ million, $\delta_t = 0^\circ$.

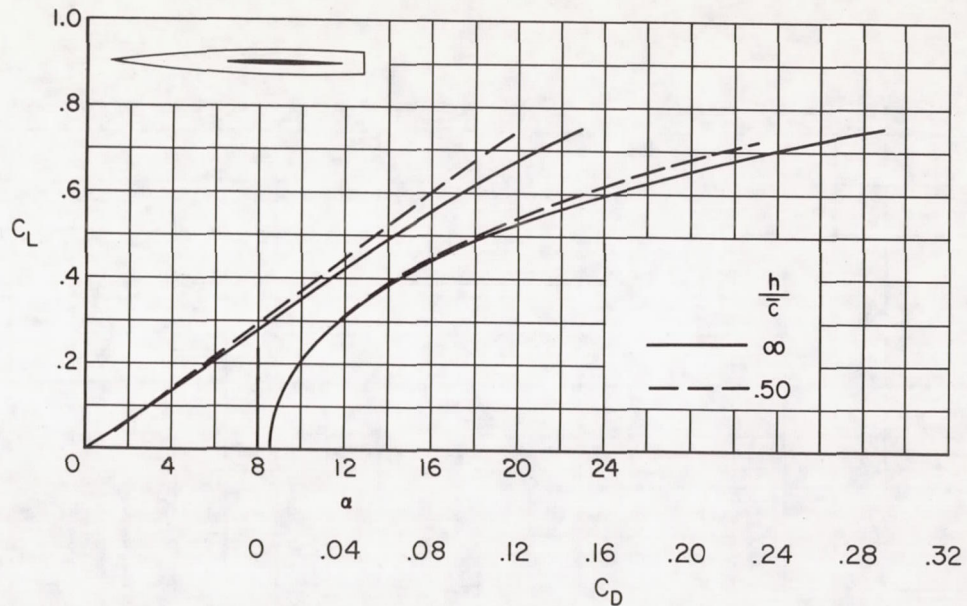


Figure 7.- The effect of ground height on the lift and drag characteristics of the tailless model in a balanced condition ($C_m = 0$); $R = 3$ million, $\delta_t = 0^\circ$.

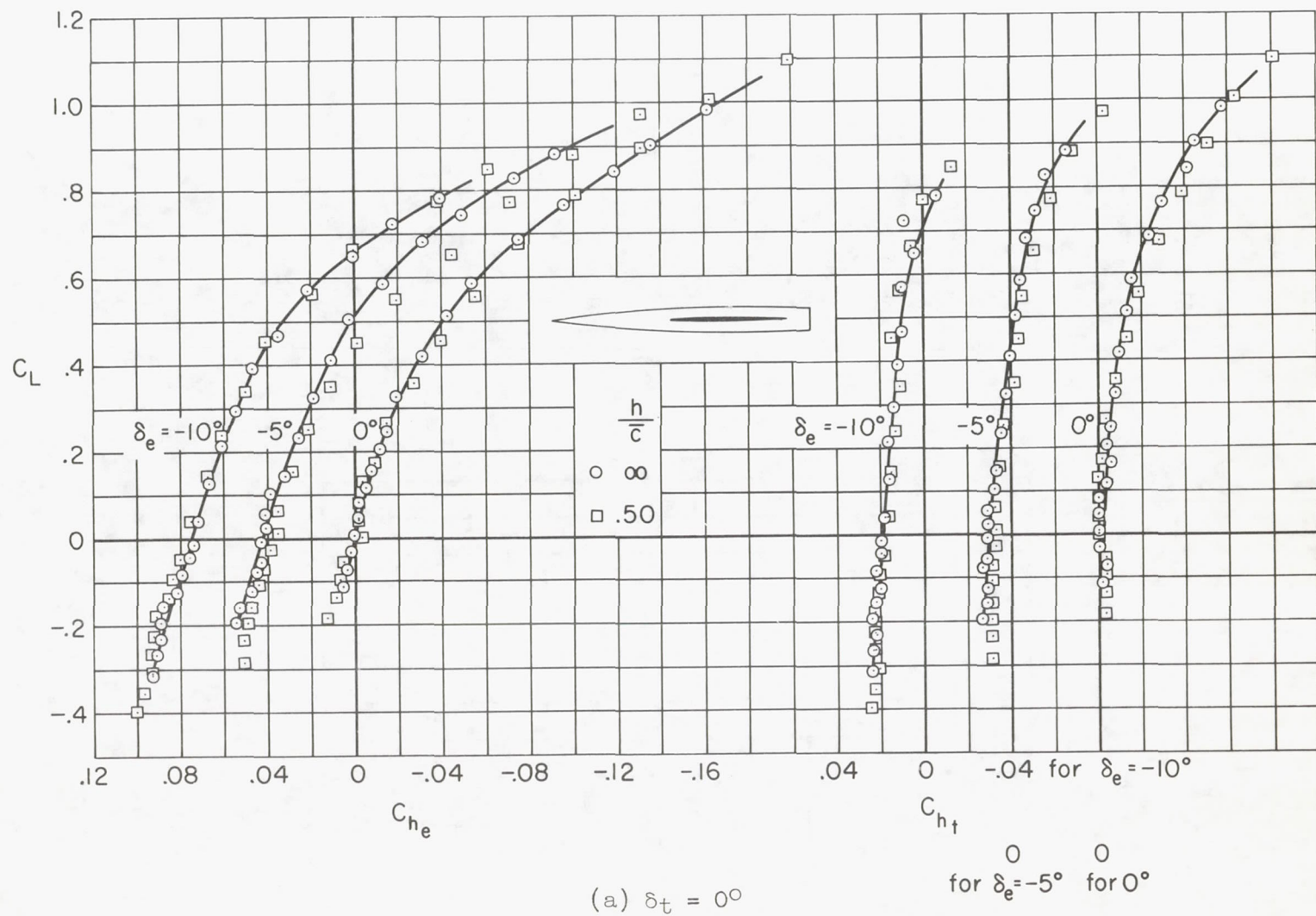


Figure 8.- The effect of ground height on the hinge-moment characteristics of the elevon and tab on the tailless model; $R = 3$ million.

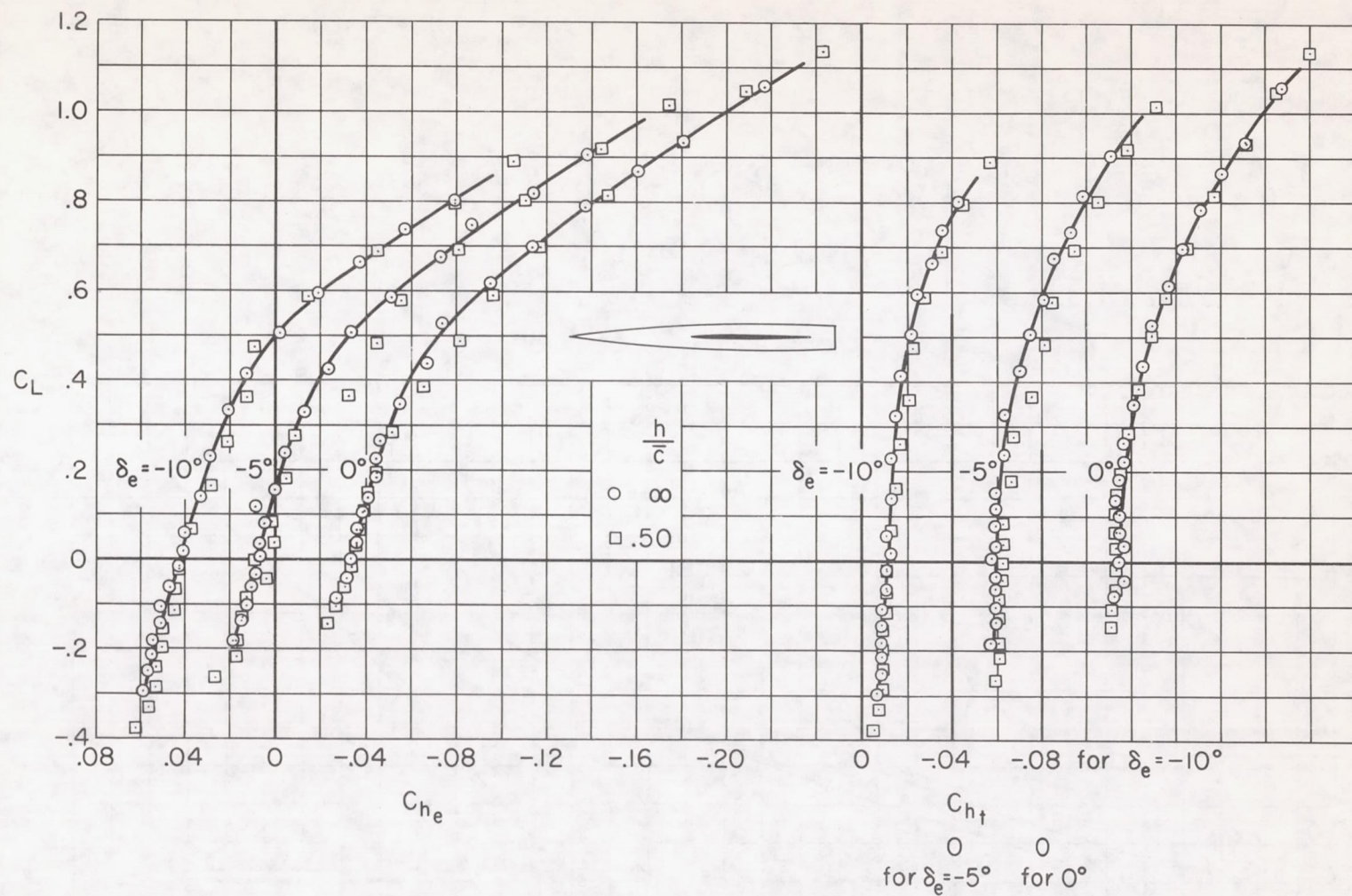
(b) $\delta_t = 5^\circ$

Figure 8.- Concluded.

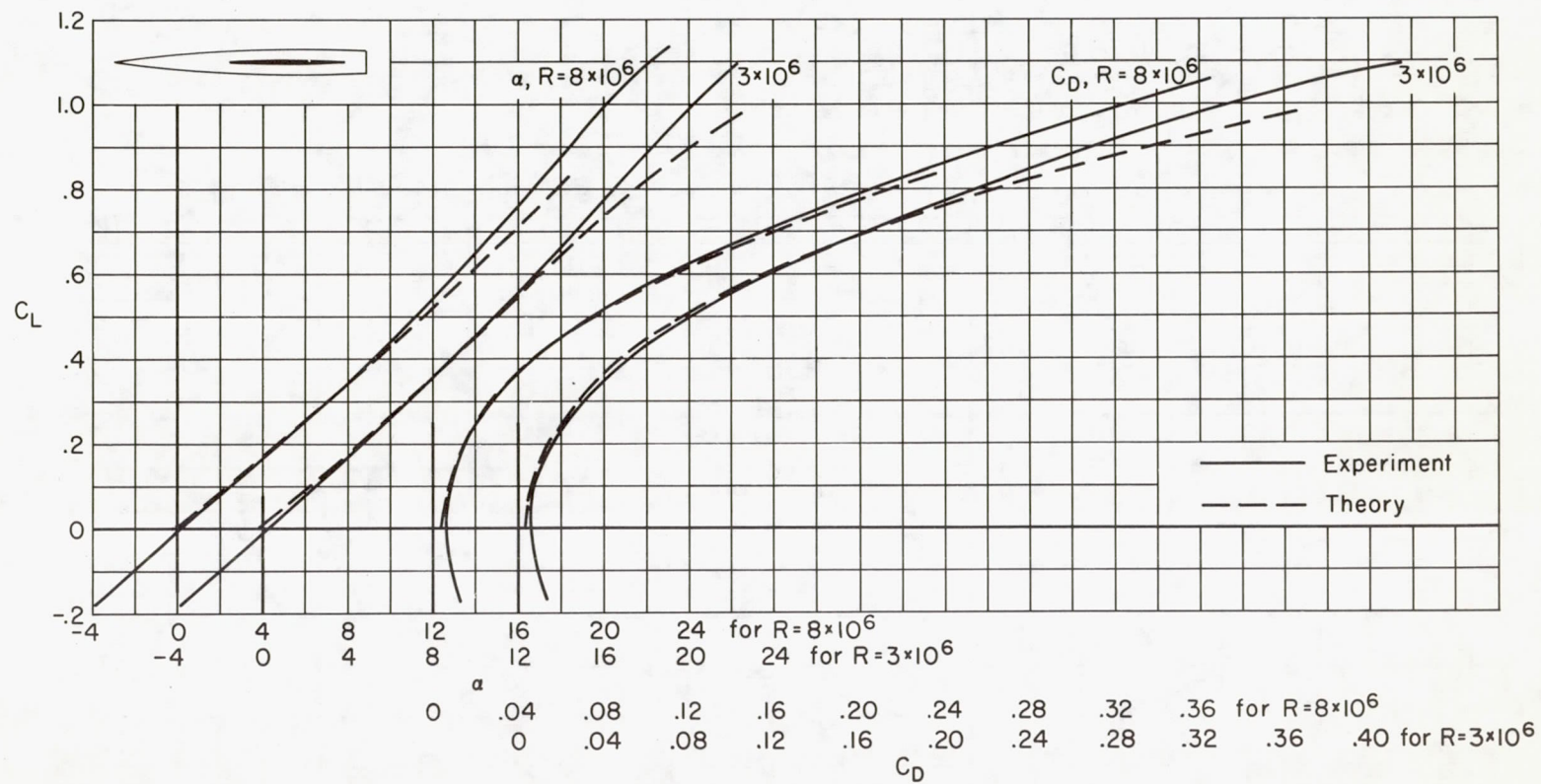


Figure 9.- A comparison between the experimental and theoretical lift and drag characteristics of the tailless model in the presence of the ground; $\delta_t = 0^\circ$, $\delta_e = 0^\circ$, $h/\bar{c} = 0.50$.

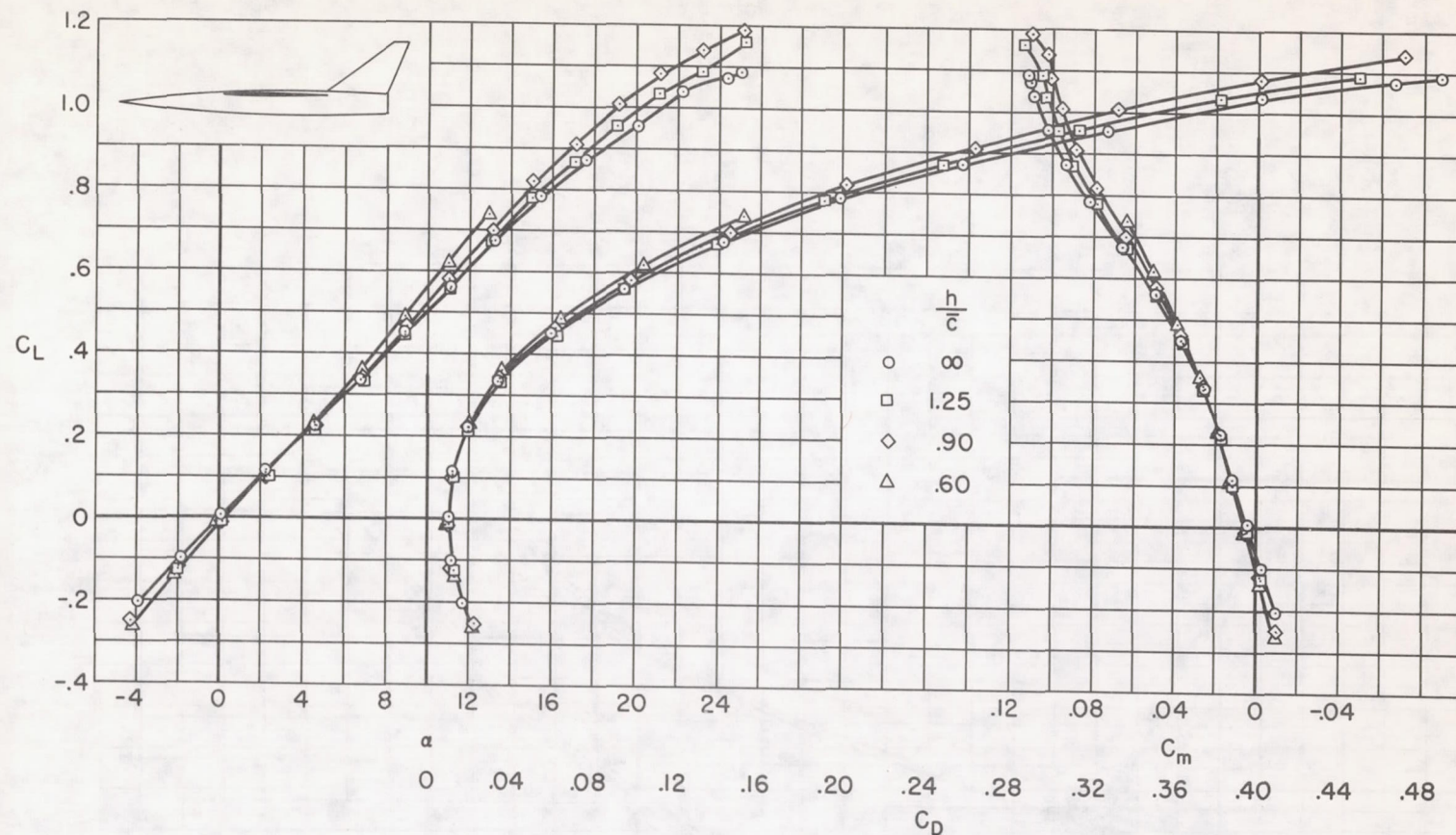


Figure 10.- The effect of ground height on the longitudinal characteristics of the tailed model;
 $R = 10$ million, $\delta_f = 0^\circ$, horizontal tail off, fuselage shortened.

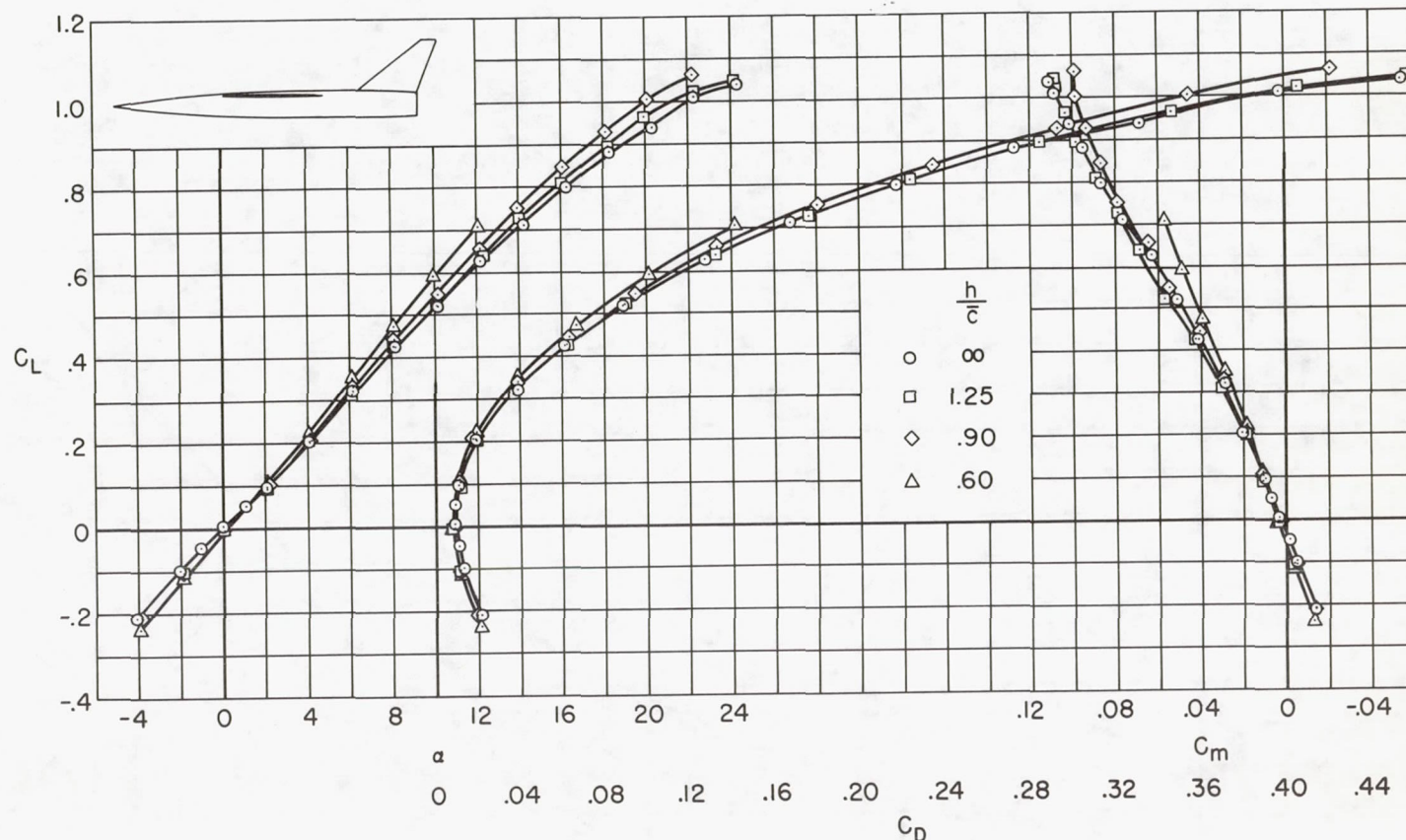
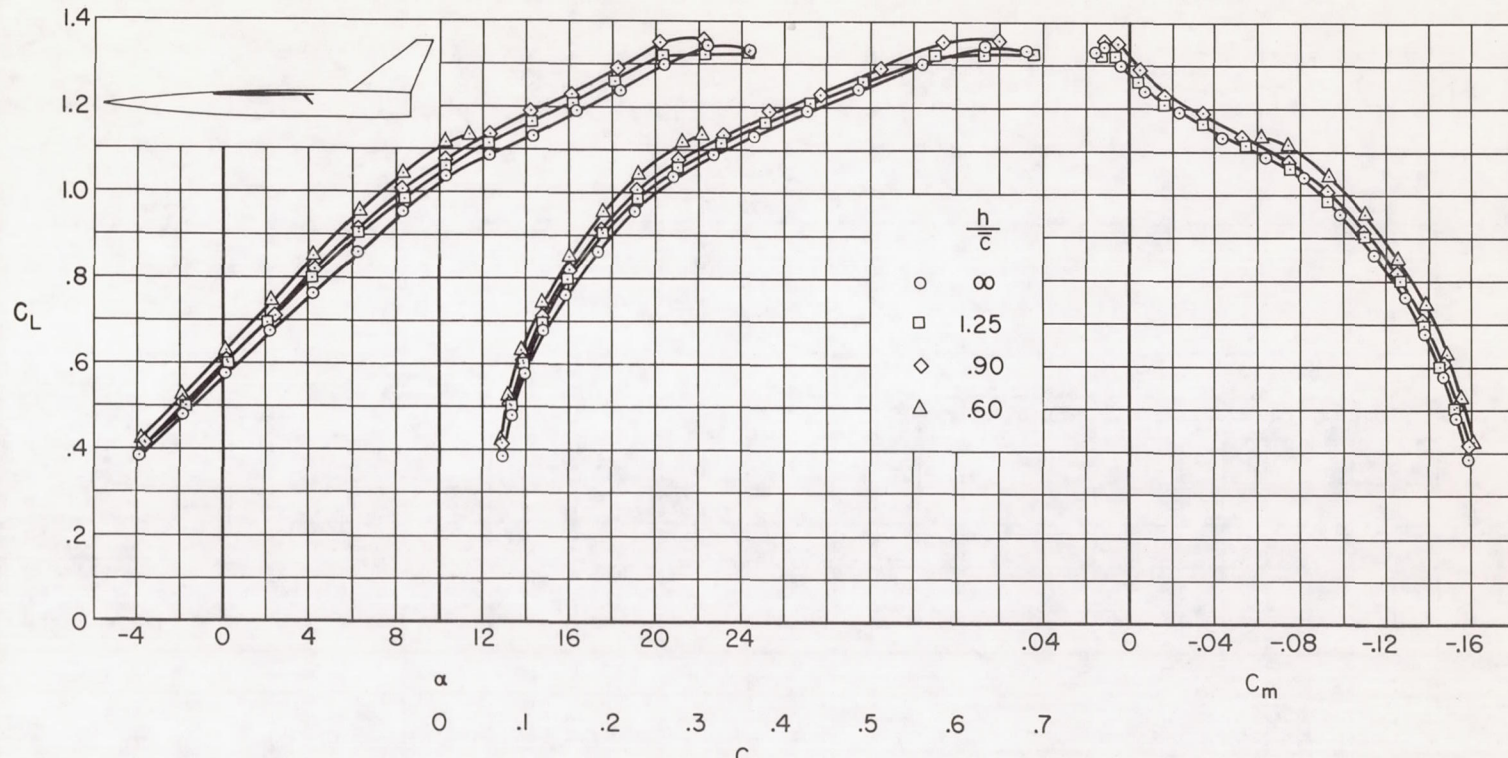
(a) $\delta_f = 0^\circ$

Figure 11.- The effect of ground height on the longitudinal characteristics of the tailed model;
 $R = 2.5$ million, horizontal tail off.



(b) $\delta_f = 40^\circ$

Figure 11.- Concluded.

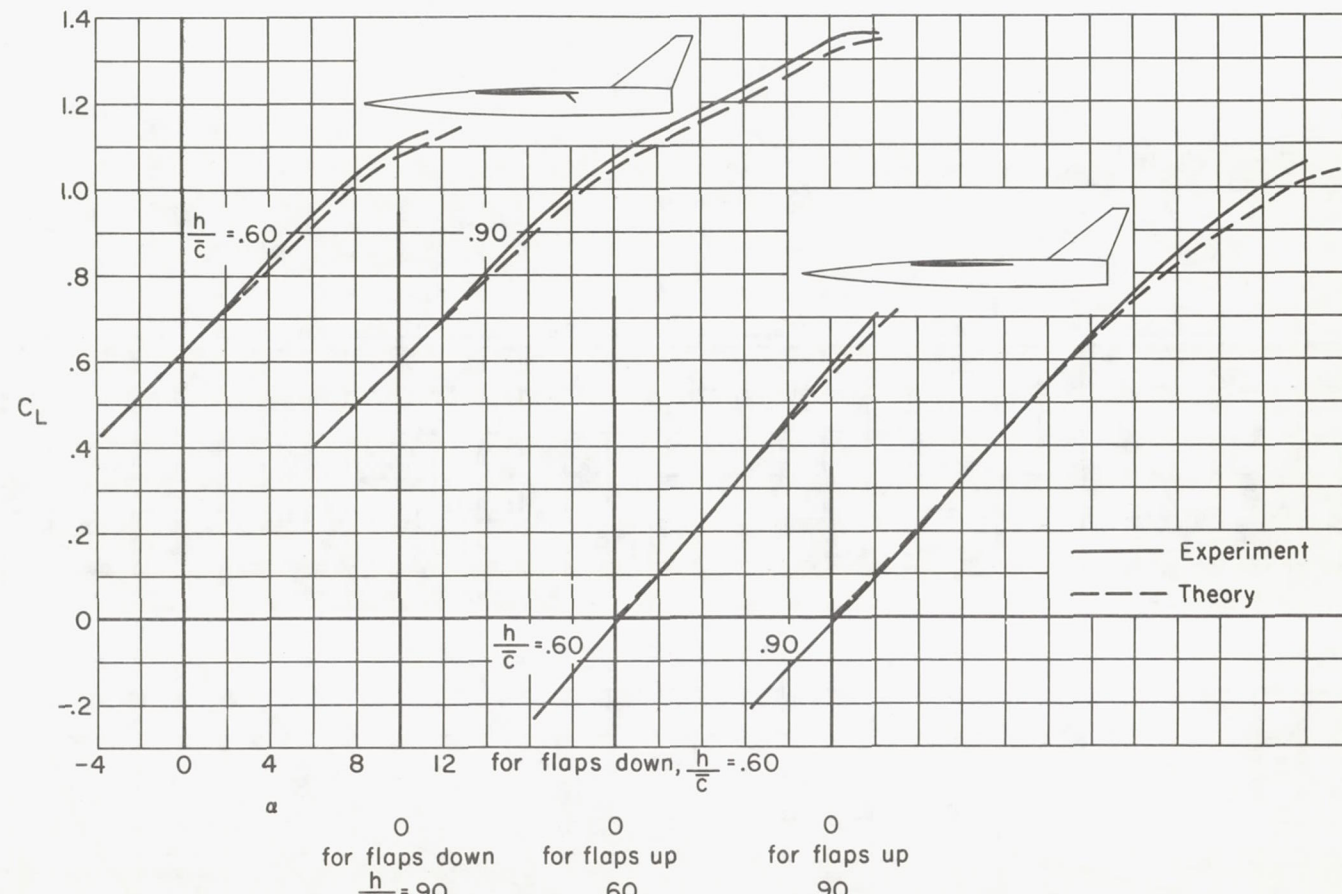
(a) C_L vs. α

Figure 12.- A comparison between the experimental and theoretical lift and drag characteristics of the tailed model in the presence of the ground; $R = 2.5$ million, horizontal tail off.

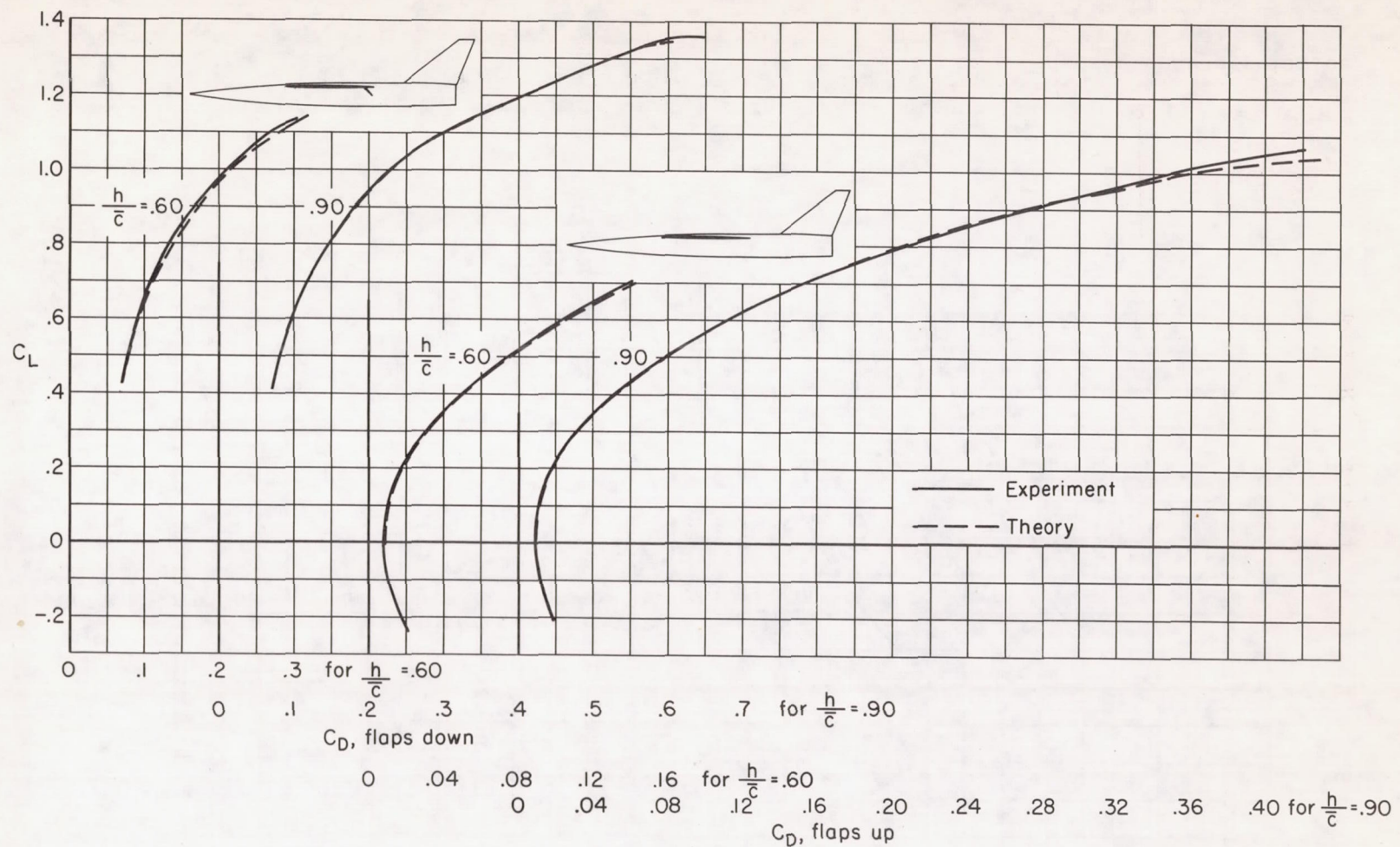
(b) C_L vs. C_D

Figure 12.- Concluded.

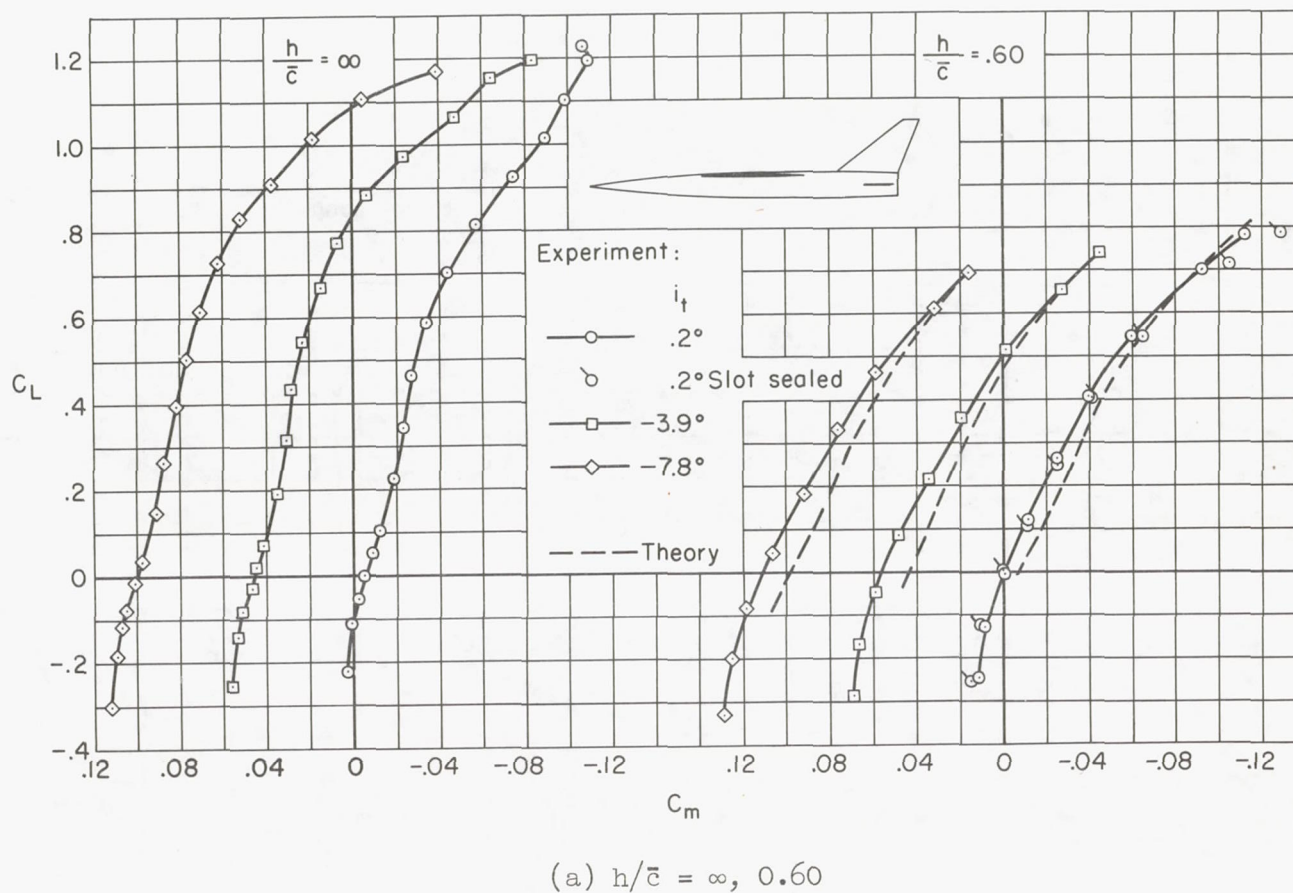


Figure 13.- The effect of tail incidence on the pitching-moment characteristics of the tailed model in the presence of the ground; $R = 2.5$ million, $\delta_f = 0^\circ$.

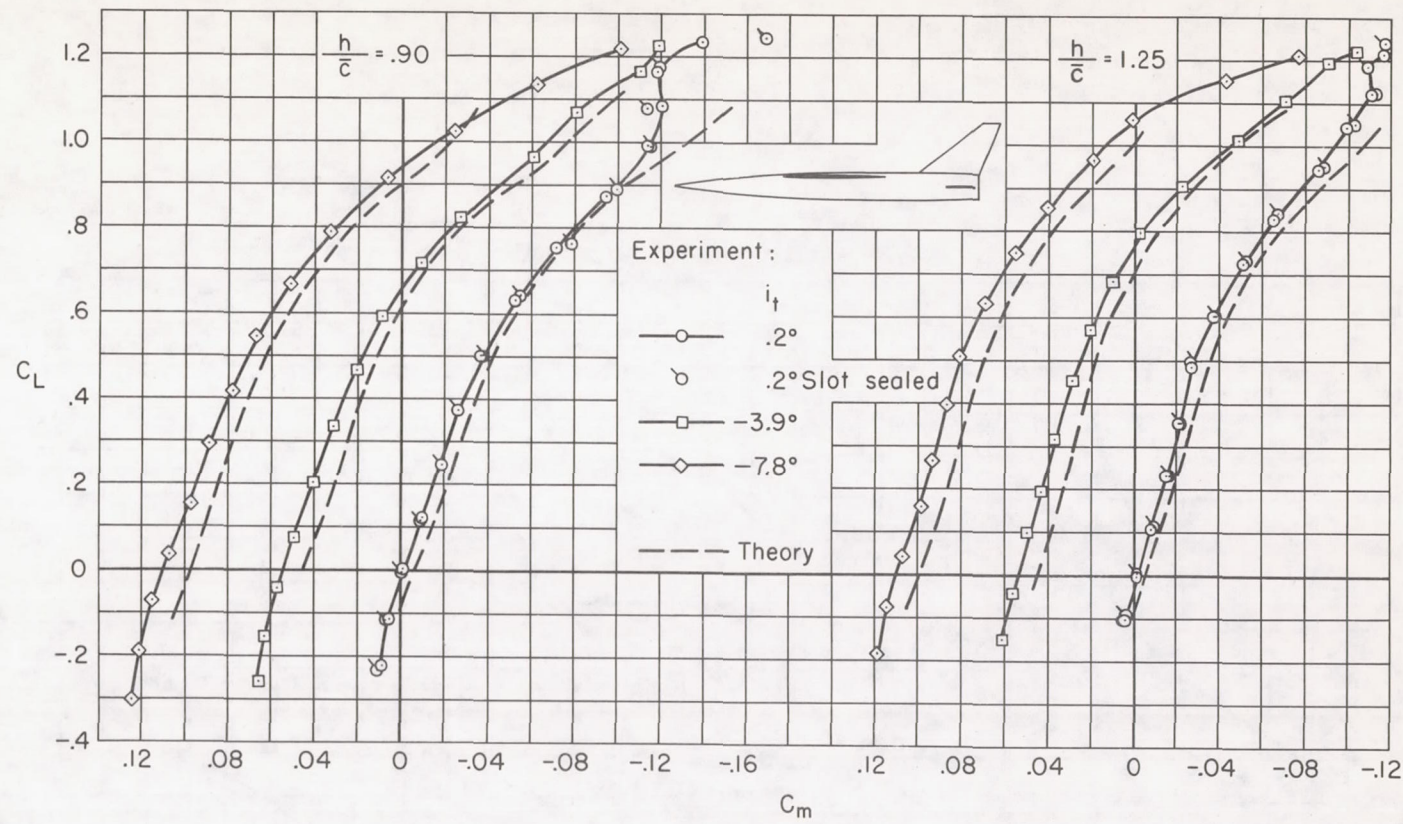
(b) $h/\bar{c} = 0.90, 1.25$

Figure 13.- Concluded.

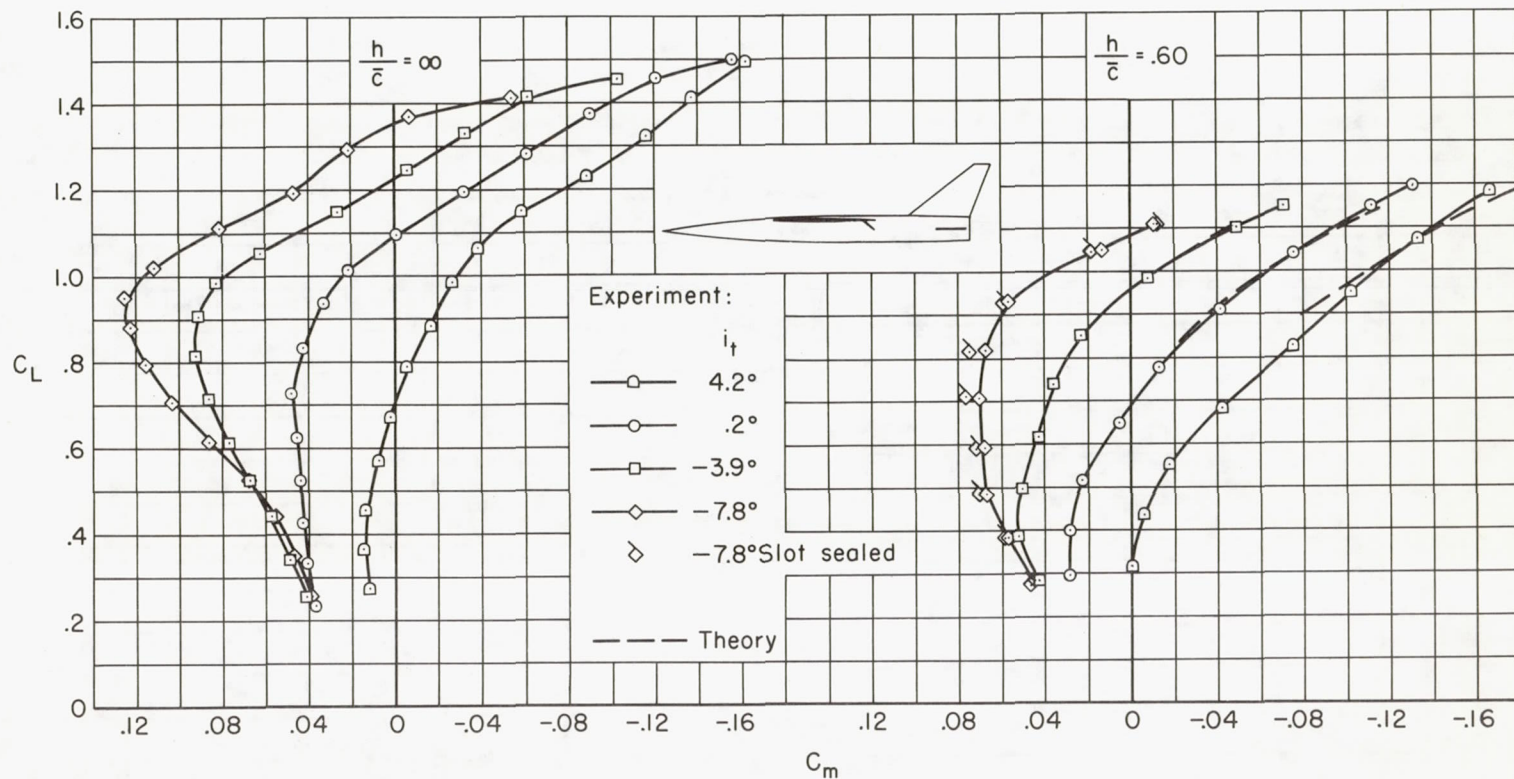
(a) $h/c = \infty, 0.60.$

Figure 14.- The effect of tail incidence on the pitching-moment characteristics of the tailed model in the presence of the ground; $R = 2.5$ million, $\delta_f = 40^\circ$.

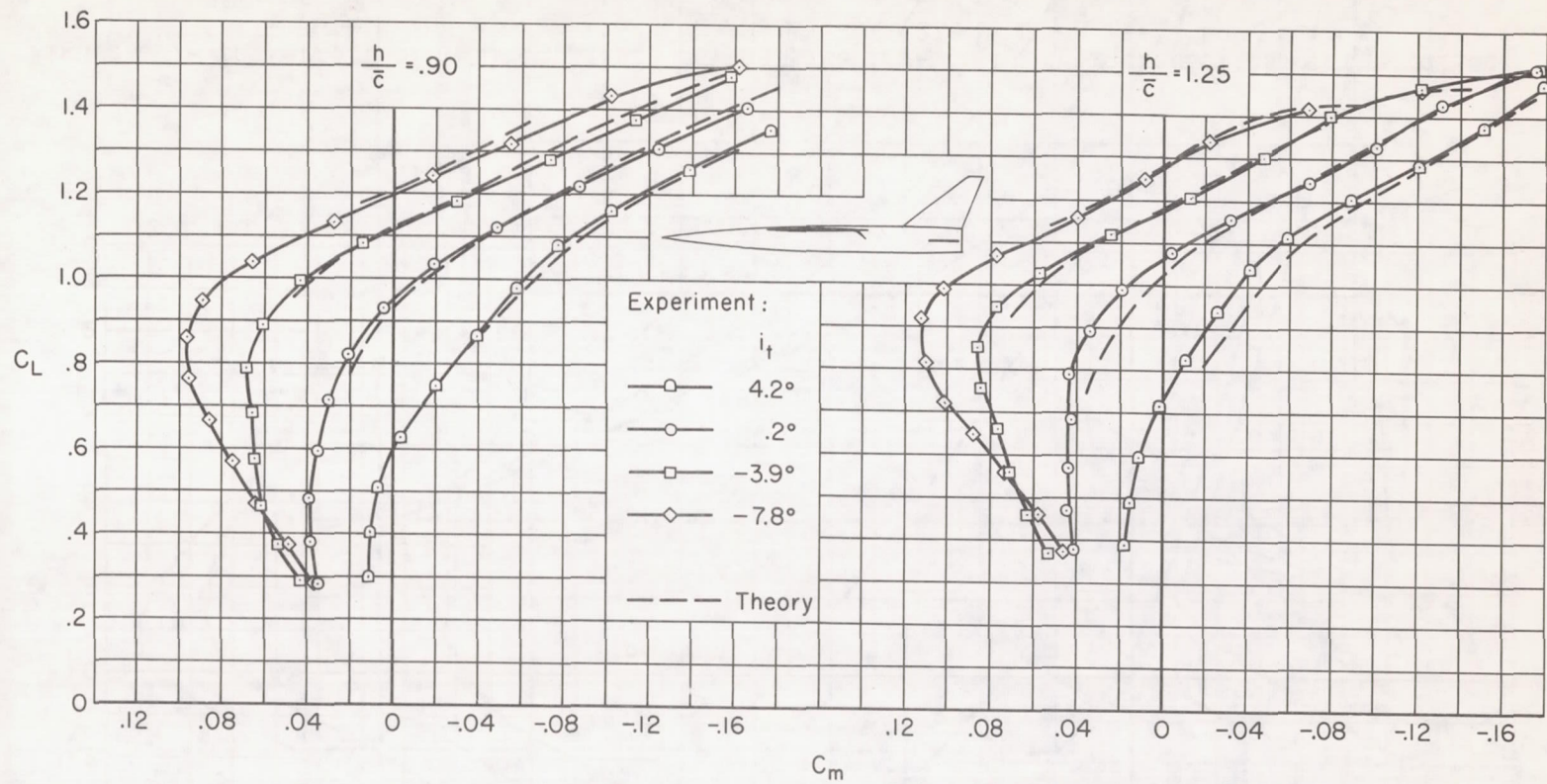
(b) $h/\bar{c} = 0.90, 1.25$

Figure 14-- Concluded.

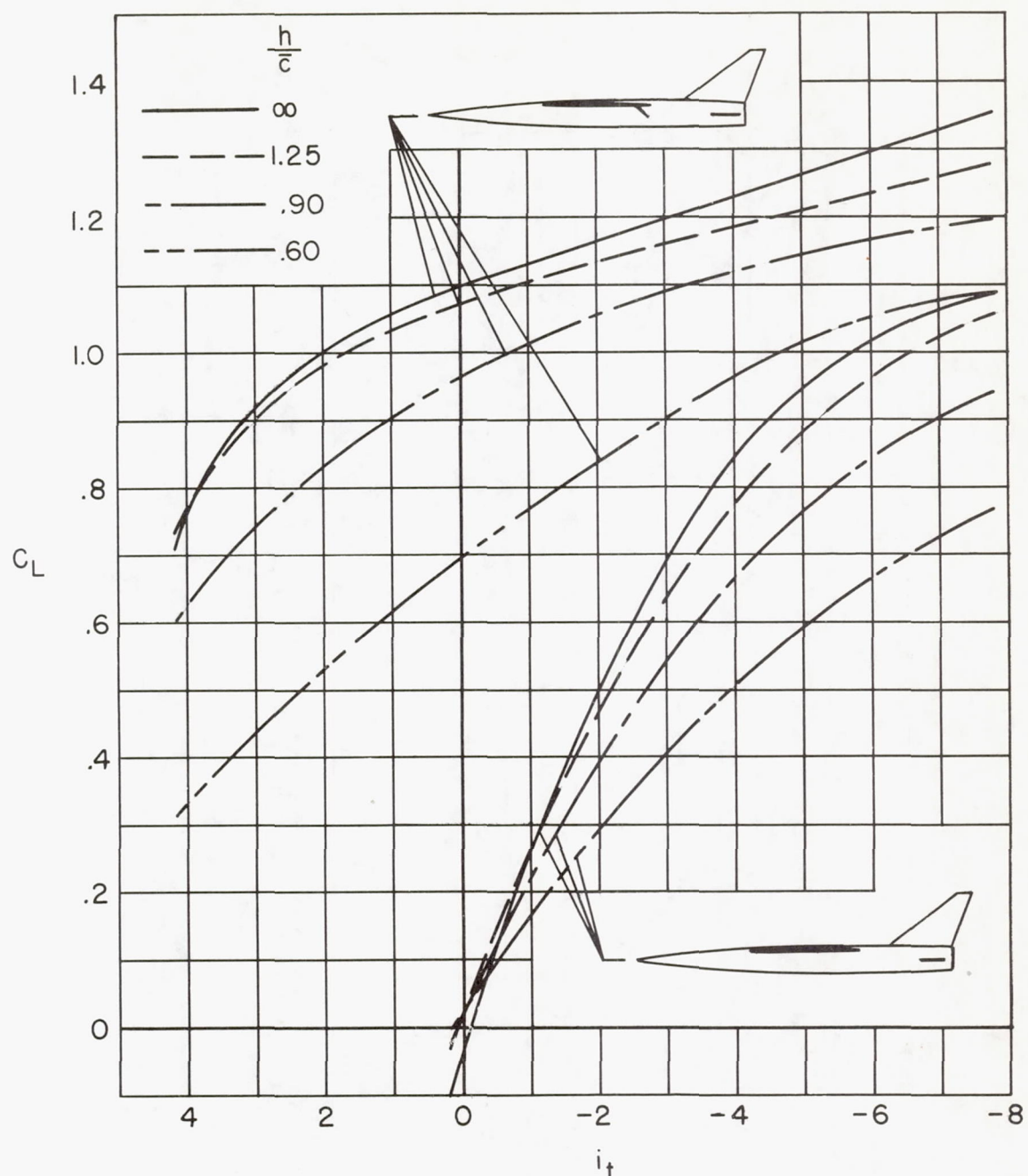


Figure 15.- The effect of ground height on the tail incidence for balance ($C_m = 0$) of the tailed model; $R = 2.5$ million.

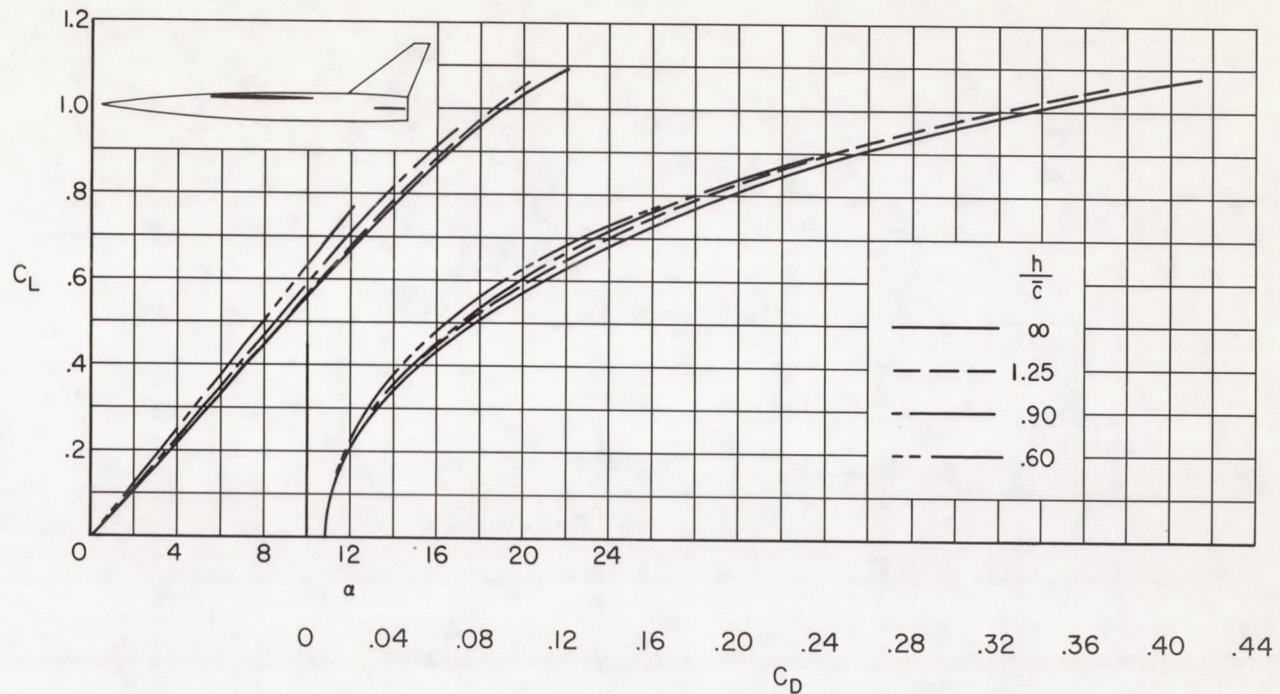
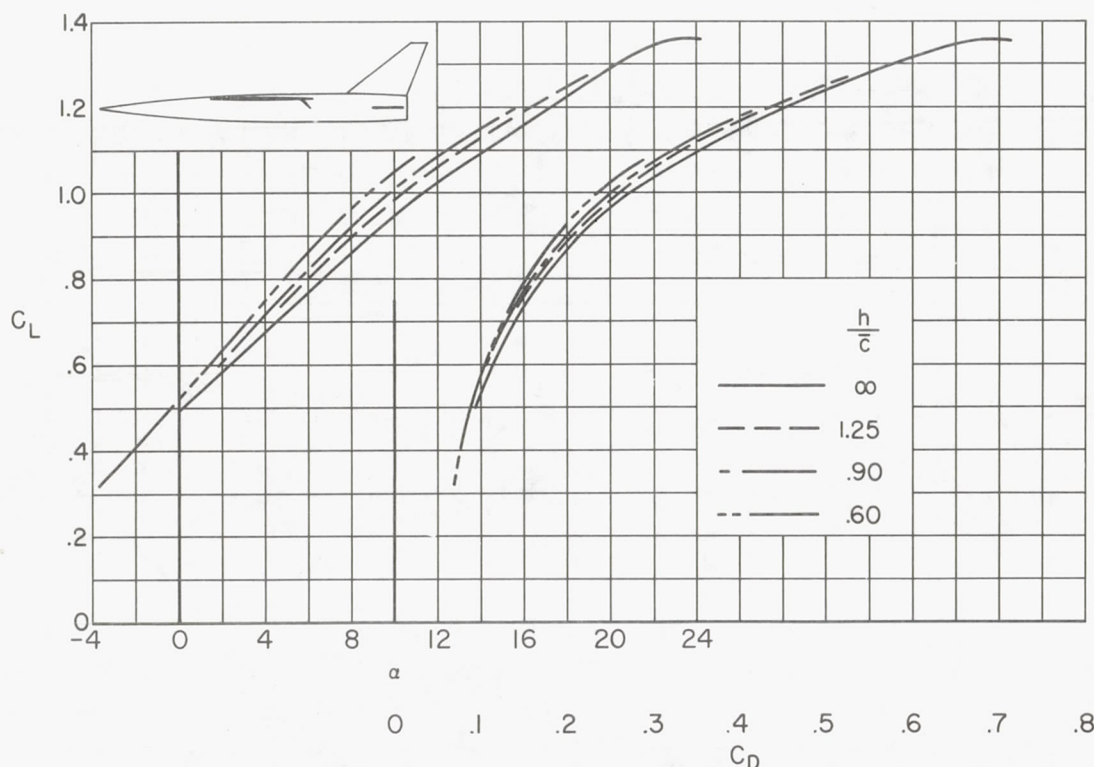
(a) $\delta_f = 0^\circ$

Figure 16.- The effect of ground height on the lift and drag characteristics of the tailed model in a balanced condition ($C_m = 0$); $R = 2.5$ million.



(b) $\delta_f = 40^\circ$

Figure 16.- Concluded.

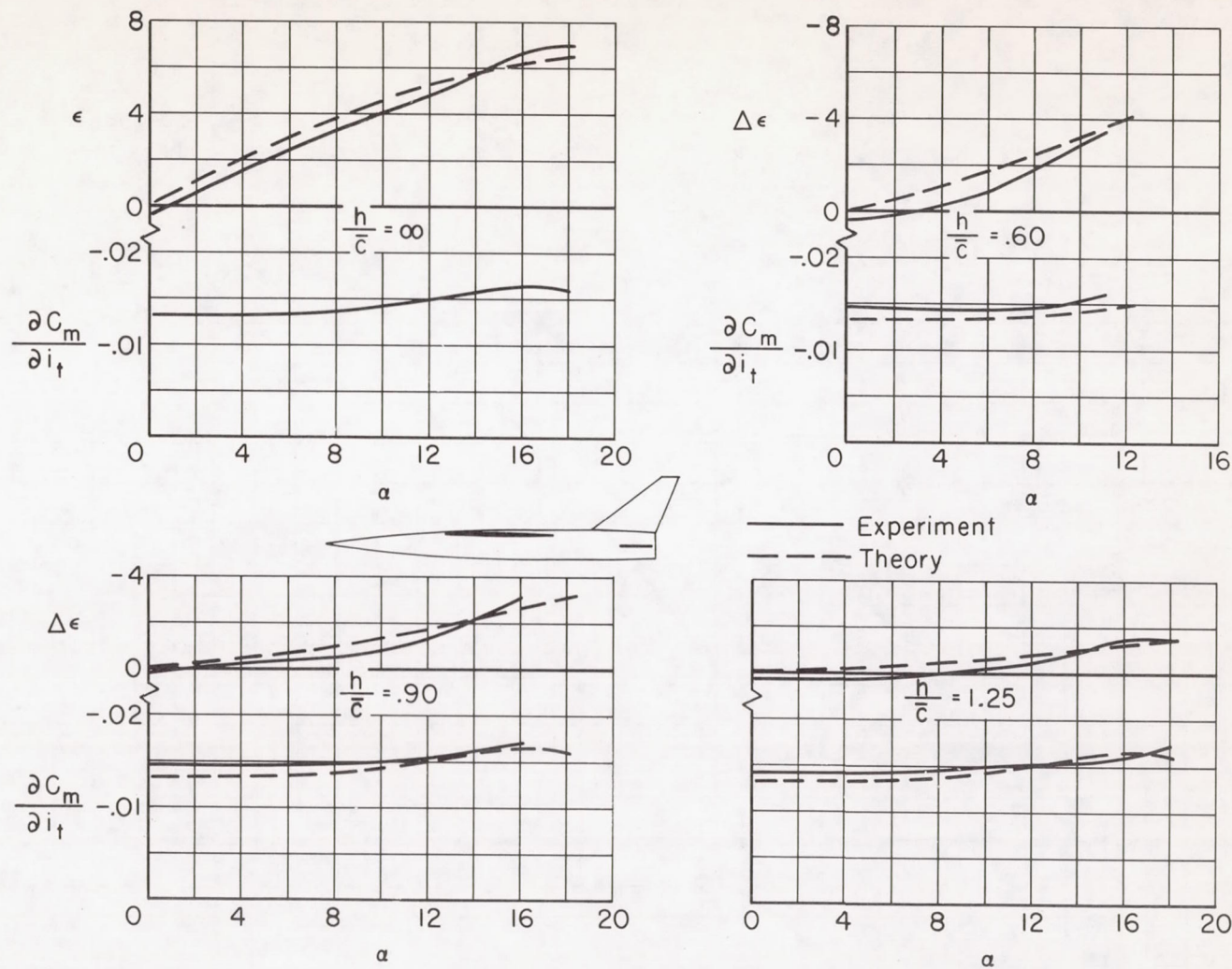


Figure 17.- A comparison between the experimental and theoretical values of the effective angle of downwash ϵ , the ground-induced change in angle of downwash $\Delta\epsilon$, and the rate of change of pitching-moment coefficient with tail incidence $\frac{\partial C_m}{\partial i_t}$ on the tailed model; $R = 2.5$ million, $\delta_f = 0^\circ$.

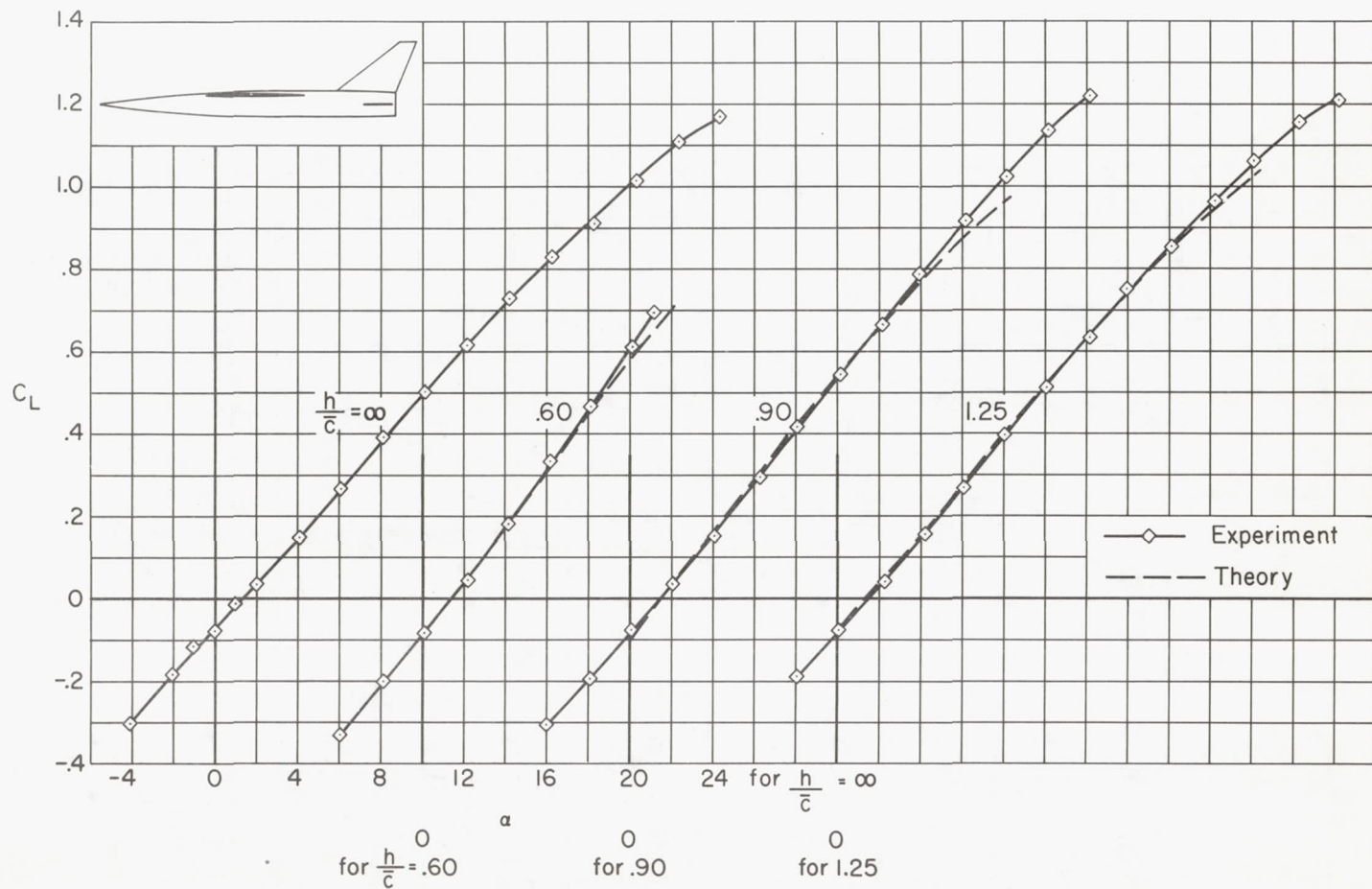


Figure 18.- A comparison between the experimental and theoretical lift characteristics of the tailed model in the presence of the ground; $R = 2.5$ million, $\delta_f = 0^\circ$, $i_t = -7.8^\circ$.

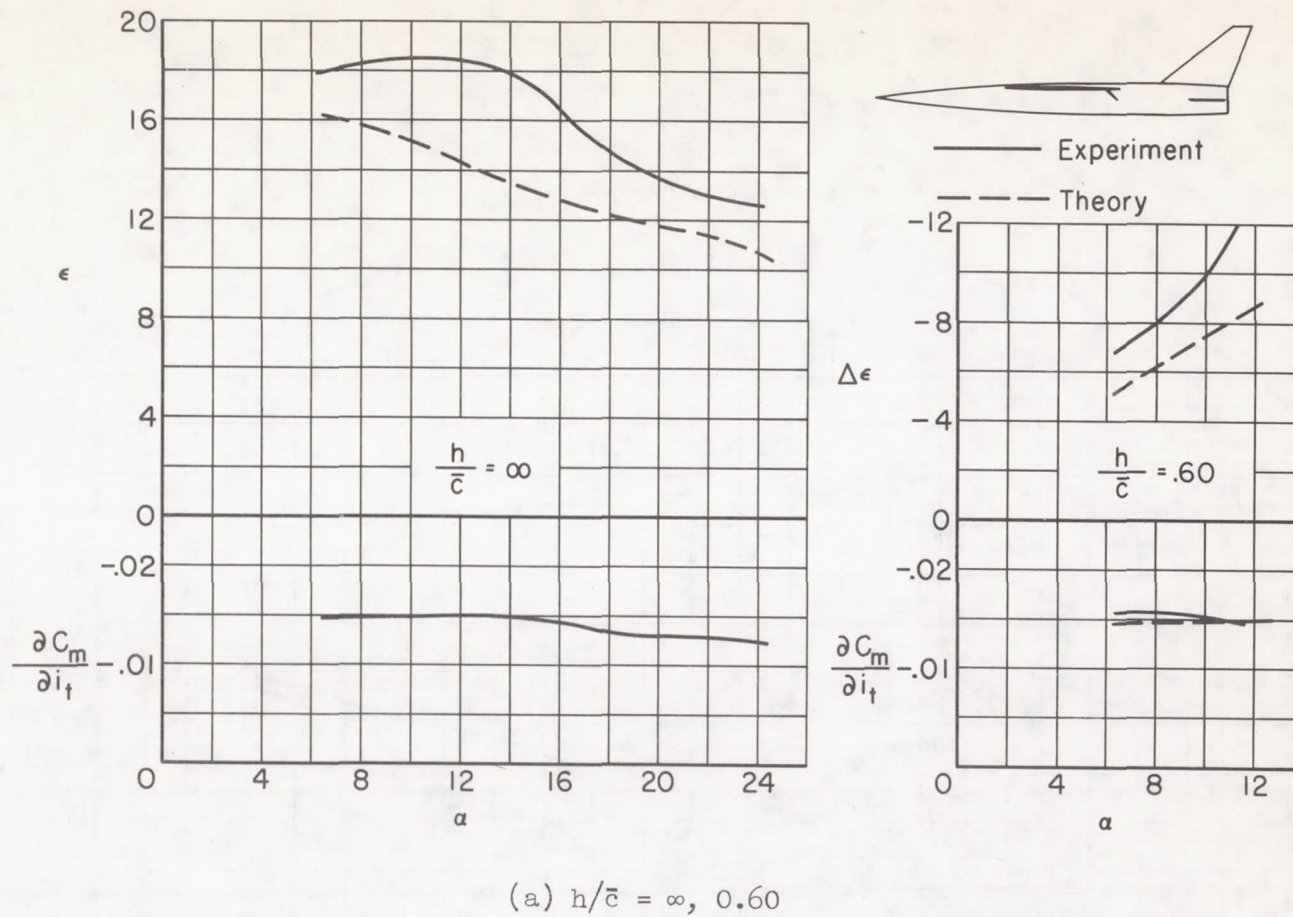
(a) $h/\bar{c} = \infty, 0.60$

Figure 19.- A comparison between the experimental and theoretical values of the effective angle of downwash ϵ , the ground-induced change in angle of downwash $\Delta\epsilon$, and the rate of change of pitching-moment coefficient with tail incidence $\partial C_m / \partial i_t$ on the tailed model; $R = 2.5$ million, $\delta_f = 40^\circ$.

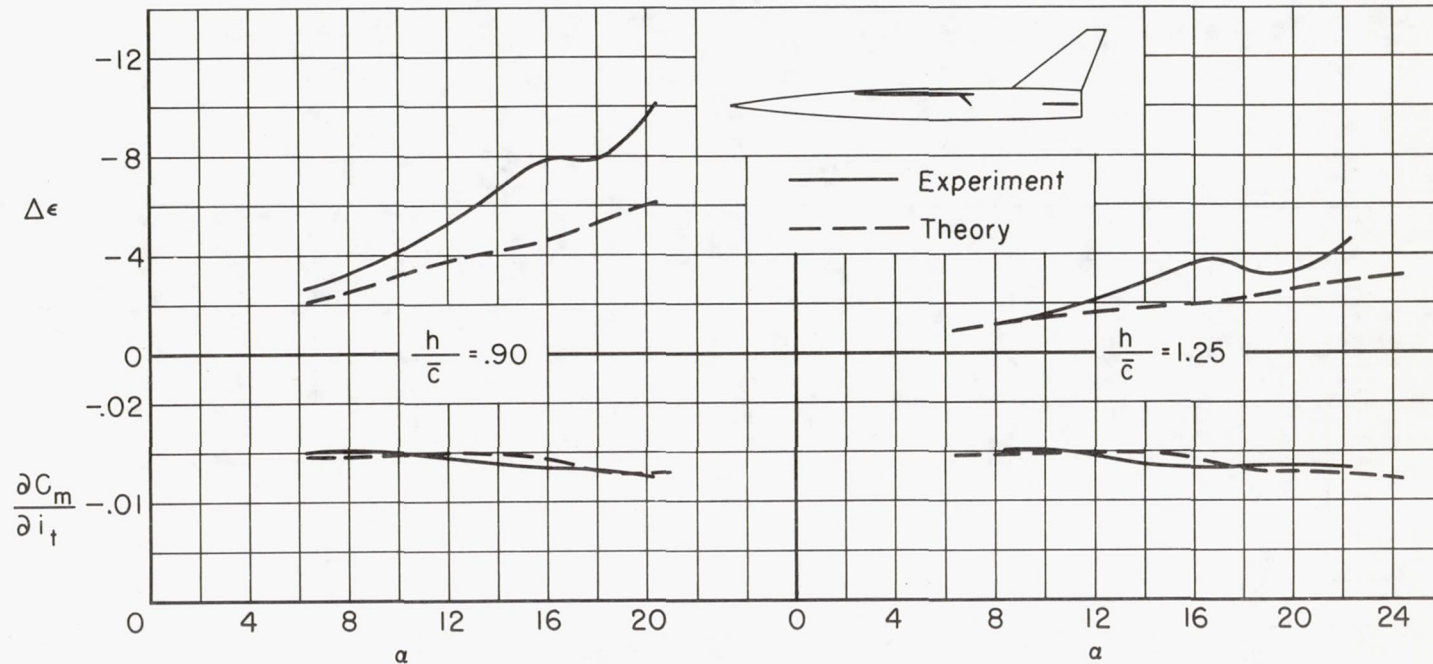
(b) $h/\bar{c} = 0.90, 1.25.$

Figure 19.- Concluded.

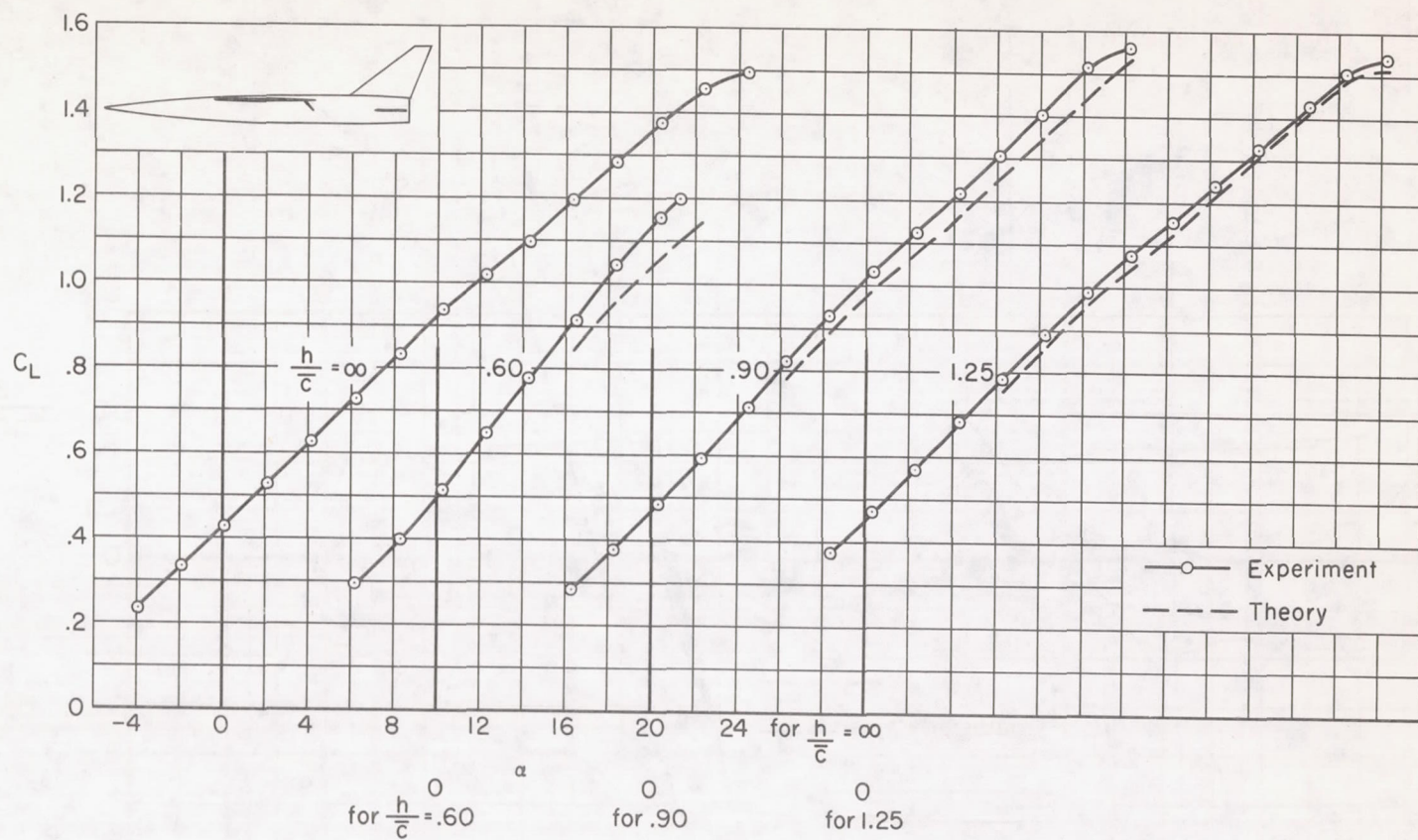


Figure 20.- A comparison between the experimental and theoretical lift characteristics of the tailed model in the presence of the ground; $R = 2.5$ million; $\delta_f = 40^\circ$, $i_t = 0.2^\circ$.

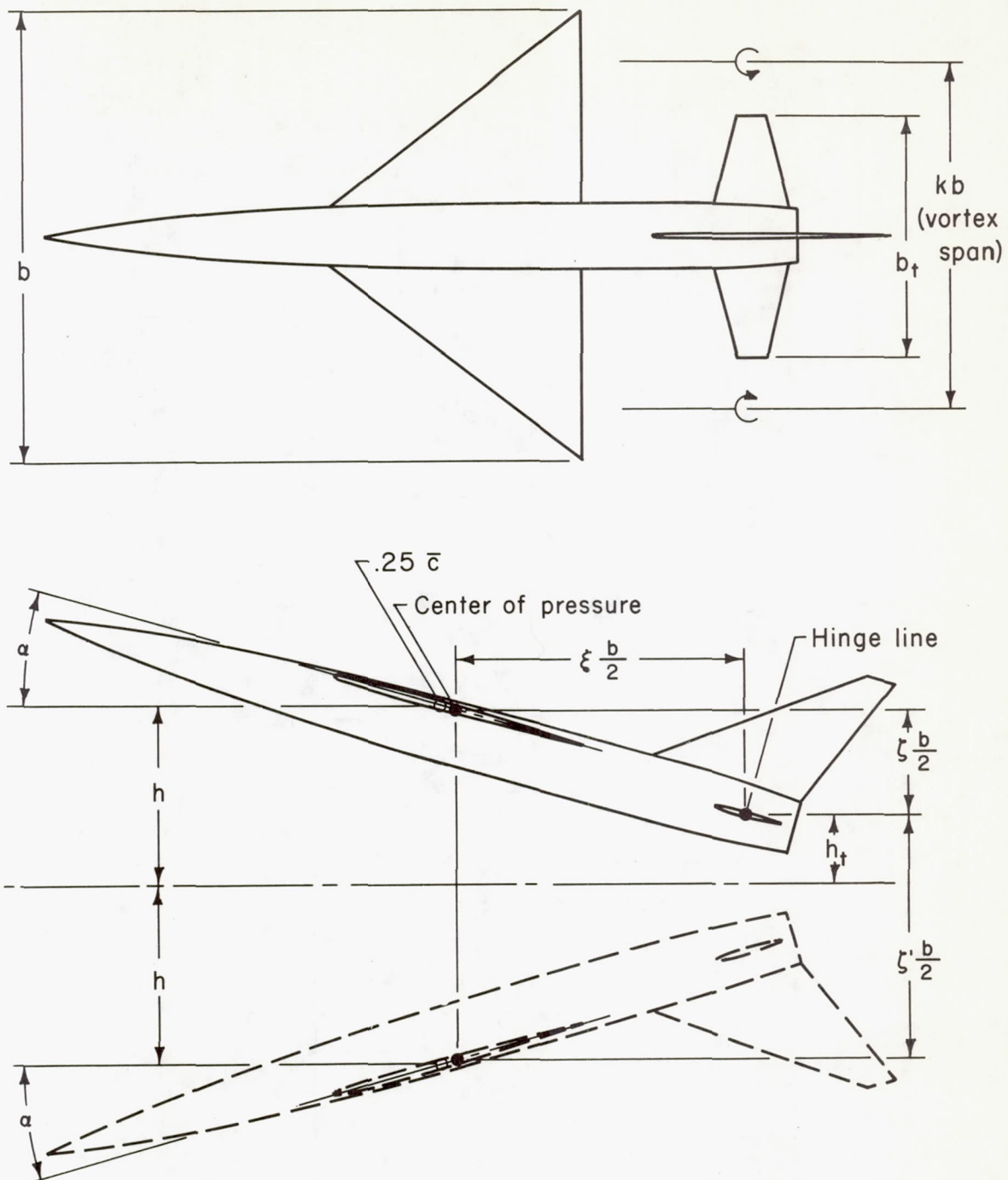


Figure 21.- Diagram of the reflection method employed in estimating ground effects.